実験室宇宙物理学の紹介：2018年青学チームの無衝突衝撃波生成実験の結果

R. Yamazaki[1], I. Miyata[1], H. Toda[1], D. Abe[1], N. Ishizaka[1], S. Kakuchi[1], R. Kawamura[1], S. Sei[1], K. Sugiyama[1], D. Suzuki[1], S. Tomita[1,7], S.J. Tanaka[1], Y. Sakawa[2], T. Sano[2], M. Ota[2], S. Egashira[2], R. Kumar[2], Y. Kuramitsu[2], K. Tomita[3], T. Morita[3], M. Edamoto[3], S. Matsukiyo[3], H. Asai[4], K. Yamazaki[4], H. Yoneda[4], N. Ohnishi[5], T. Umeda[6], Y. Ohira[7], A. Ishii[7], T. Takezaki[8]

[1] Aoyama Gakuin University, [2] Osaka University, [3] Kyushu University, [4] University of Electro-communications, [5] Tohoku University, [6] Nagoya University, [7] University of Tokyo, [8]National Institute of Technology, Kitakyushu College

実験室宇宙物理学

・(現場にいくのが不可能な)宇宙空間で起こる現象・物理過程を地球上で再現する。

＝＞　宇宙空間で起こる現象とは対照的に

・制御可能: 好きな状況を作れる。

・「その場」観測により豊富なデータが得られる。

実験室宇宙物理の発展により

・未解明の現象・物理過程を理解できるかもしれない。

・新たな天体現象を予言できるかもしれない。

・予想もしなかった物理現象の発見につながるかもしれない。

天文観測、理論計算・シミュレーションに続く第3の独立な研究ツールとしたい！

実験室宇宙物理学

今回は大型レーザーを用いた衝撃波実験の紹介がメインだが、

実験室宇宙物理はレーザー実験が全てではない。
例： MRI, SASI, Shocks…

大型レーザー(NIF, OMEGA,…)を使った実験の例：
EOS測定,
リコネクション,
jet伝播,
磁気乱流(ダイナモ, 乱流中での粒子拡散),
プラズマ不安定(current instabilities, Bell instability,…)

Experimental parameters

Parameters of unshocked plasma:

$n_e \sim n_i \sim 10^{18}\text{cm}^{-3}$, $T_e \sim T_i \sim 100$ eV, $B \sim 1$ T

=> plasma parameter: $n_e \lambda_{De}^3 \sim 4 \times 10^2$ ($\propto n^{-1/2} T^{3/2}$)

electron skin depth: $c/\omega_{pe} \sim 10^{-3}$ mm ($\propto n^{-1/2}$)

plasma beta: $\beta \sim 40$ ($\propto n T B^{-2}$)

freq. ratio: $\omega_{pe}/\omega_{ce} \sim 3 \times 10^2$ ($\propto n^{1/2} B^{-1}$)

Alfven velocity: $v_A \sim 2 \times 10^6$ cm/s ($\propto n^{-1/2} B$)

sound velocity: $c_s \sim 10^7$cm/s ($\propto T_i^{1/2}$)

gyro radius of thermal *e*'s : $r_{g,e} \sim 10^{-2}$ mm ($\propto T_e^{1/2} B^{-1}$)

gyro radius of thermal ions: $r_{g,i} \sim 1$ mm ($\propto T_i^{1/2} B^{-1}$)

=> For $M_s \sim 10$ ($v_s \sim 10^8$cm/s, $M_A \sim 50$),

downstream temp.(simply by RH): $T_d \sim 32\, T_u \sim 3$ keV

=> required system size > 1cm. or B >> 1T ?

Ion mean free path for Coulomb collision:

$$\lambda_{ii} = \frac{m_p^2 v_{sh}^2}{8\pi n_0 Z^4 e^4 \ln\Lambda} = 7.0 \times 10^{18}\mathrm{cm}\ \frac{v_8^4}{Z^4 n_0}\left(\frac{\ln\Lambda}{30}\right)^{-1}$$

$$\ln\Lambda = \ln\left[\frac{m_p v_{sh}^2}{Z^2 e^2}\sqrt{\frac{kT_0}{4\pi n_0 e^2}}\right] = 32 + \ln\left[(v_8/Z)^2\sqrt{T_{eV}/n_0}\right]$$

レーザープラズマの業界の「collisionless (shock)」の定義：

この λ_{ii} が system size (または衝撃波遷移層)よりも大きいときcollisionless。

レーザープラズマの人たちのプレゼンをきくときは、
宇宙物理・天体物理の業界の定義とは異なることに注意が必要。

銀河団、超新星残骸、太陽風、実験室の衝撃波で、マッハ数と特徴的長さの大小関係はどれも同じ:

	n_0 (cm^{-3})	T_0 (K)	v_{sh} ($\mathrm{cm\ s}^{-1}$)	B_0 (μG)	$L_{\rm sys}$ (cm)	$\Delta_{\rm obs}$ (cm)	λ_{ii} (cm)	$r_{g,i}$ (cm)	L_i (cm)	ω_{pe}/ω_{ce}	β	M_A	M_s	M_{el}
Clusters	10^{-3}	10^8	10^8	1	10^{25}	10^{22}	10^{22}	10^{10}	10^9	10^2	10^2	10	1	10^{-2}
SNRs	1	10^4	10^8	10	10^{19}	10^{16}	10^{19}	10^9	10^7	10^2	1	10^3	10^2	1
SW (TS)	10^{-3}	10^5	10^8	0.1	10^{15}	10^9	10^{22}	10^{10}	10^9	10^2	1	10	10	1
SW (1 AU)	10	10^5	10^8	10	10^{12}	10^6	10^{19}	10^9	10^7	10^2	1	10^2	10	1
Laboratories	10^{17}	10^5	10^8	$< 10^{10}$	1	10^{-3}	10^2	> 1	10^{-1}	$> 10^2$	< 1	10	10	1

$$M_{el} < M_s \leq M_A$$

$$L_i < r_{g,i} \ll \lambda_{ii}$$

ついでに　どの場合も、プラズマ $\beta \sim \mathrm{O}(1)$.

$M_{\rm el}$: electronic sonic Mach number,
$M_{\rm s}$: sonic Mach Number,
$M_{\rm A}$: Alfven Mach number,

$L_{\rm i}$: ion skin depth,
$r_{\rm g,i}$: ion gyro radius,
λ_{ii} : ion Coulomb m.f.p.

Collisionless shocks are ubiquitous

Shocks

* are ubiquitous in various astrophysical, heliospheric, and laboratory plasmas.
  --- examples will be shown later !

* arise when two counter-streaming supersonic flows interact.

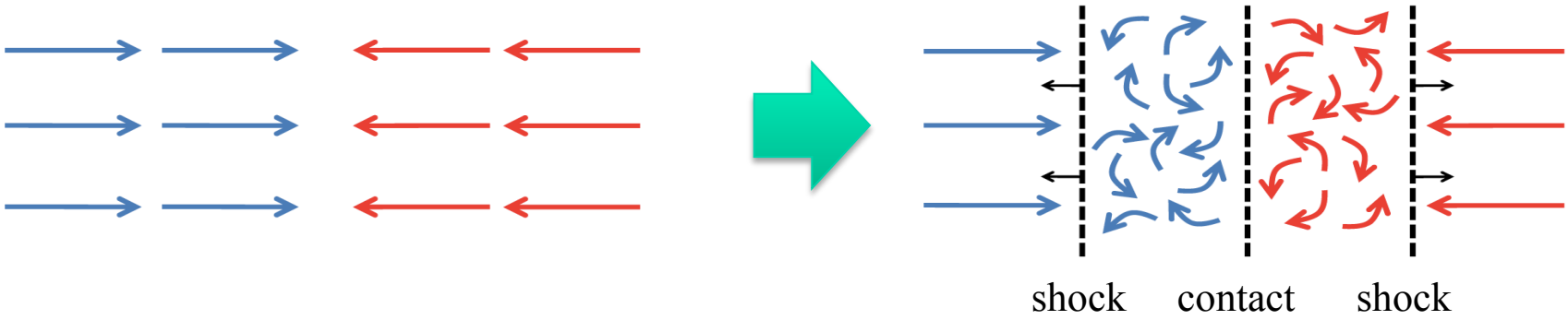

* are, in most cases, "collisionless" mainly because of low-density:
  --- Coulomb mean-free-path is much larger than the system size.
  --- Particle distribution NOT going to perfect Maxwelian.
  --- Various components arise during dissipation process.

* consist of multi-scale physics:
  --- electron/ion kinetic scales (<< size of objects) are important for dissipation.
  --- all scales are nonlinearly coupled (e.g., Umeda, RY+11)

Unsolved problems on shock physics

* Dissipation mechanism of the collisionless shocks:
  --- gas heating mechanism ? (T_e, T_i just downstream ?)
  --- energy partition among various components (e, i, B, rela, waves, turb,…) ?

* Shock structure:
  --- electron scale waves?
  --- ion scale: ripples, shock reformation?
  --- back reactions of accelerated particles (=> shock modification) ?

* Injection to Fermi acceleration process:
  --- particle acceleration is one of dissipation mechanisms !
  --- injection rate?

All these processes may be coupled !

How do the above processes depend on upstream conditions ?
  --- Mach numbers (M_A, M_s, M_{el})
  --- plasma β
  --- shock angle
  --- ionization fraction

PIC simulation for low-M shocks

Our simulation studies on electron acceleration.

Umeda, RY+ (2009)

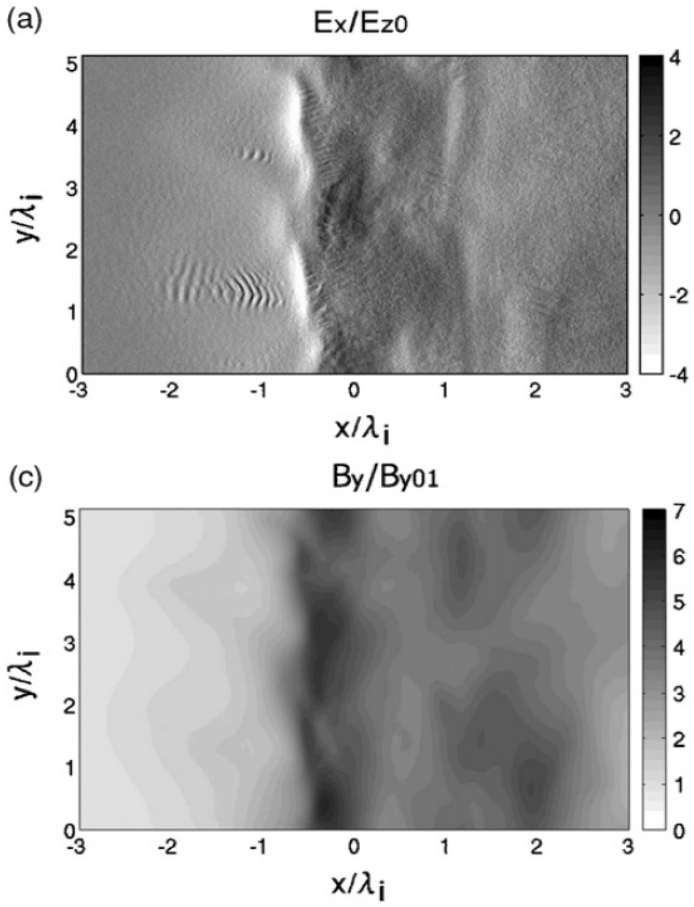

Surfing acceleration by ESW emitted by shock ripple.

Matsukiyo, Umeda, RY + (2012)

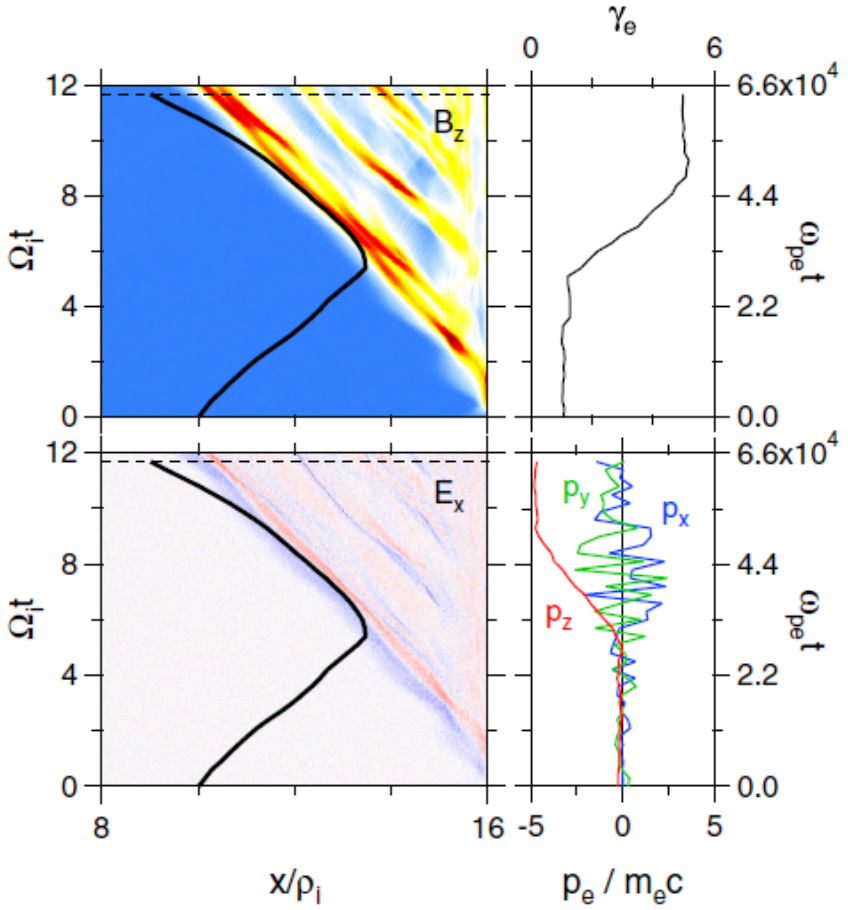

Shock drift acceleration
in high-beta case, seen in cluster shocks.

Low-Mach-number shocks

Low-Mach-number shocks can be seen in

* solar-terrestrial shocks,
* old supernova remnants,
* largest-scale (> mega light years!) cluster shocks,

… they exist even young supernova remnant shocks (CR modified shocks).

Problems of low-Mach number shocks

* Does particle acceleration occur?
  --- particle injection above "1st critical Alfven Mach number (~3)" ?
  Shock structure drastically changes across M_{crit}.
  --- for supercritical shocks, incoming ions are reflected.
  (=> wave excitation => particle scattering => acceleration?).
* Shock structure is nonstational ?
  --- shock reformation, ripples
  --- coupled with particle reflection process
* How the above processes depend on shock parameters (M_s, β, Θ_B, …)

Critical Mach numbers

1st Critical Mach number M_{crit} :

No smooth transition if $M_A > M_{crit}$ (1-fluid MHD).

A part of incoming ions is reflected by shock electrostatic potential.

Whistler Critical Mach number M^{w}_{crit} (Kennel et al. 1985) :

Whistler waves cannot propagate upstream if $M_A > M^{w}_{crit}$ (i+e 2-fluid system).

$$M^{w}_{crit} \sim \frac{\cos\theta_{Bn}}{2}\sqrt{\frac{m_i}{m_e}}$$

3rd Critical Mach number M^{inj}_{crit} (Amano & Hoshino 2010)

Whistler waves, which scatter electrons leading to injection, are not damped by electron cyclotron damping if $M_A > M^{inj}_{crit}$.

$$M^{inj}_{crit} = \frac{\cos\theta_{Bn}}{2}\sqrt{\frac{m_i}{m_e}\beta_e}$$

=> defining the critical Mach number for electron injection ? (Amano & Hoshino 10)

How to study (low-M) shocks?

* (1) Observations
  --- remote sensing : e.g., cluster shocks by radio ~ X-ray ~ γ-ray
  --- in-situ : e.g., Earth's bow shock

* (2-1) Theoretical works
  --- radiation mechanisms => estimate the amount of nonthermal particles:
  (e.g., electron injection rate by cluster optical inverse Compton (e.g., RY & Loeb15)
  --- simple fluid approximation => energetics (e.g., Vink & RY 15)
  --- linear analysis for kinetic processes => wave excitation mechanism

  (2-2) Kinetic simulations
  --- Particle-in-cell simulations: from electron to ion scale
  --- Hybrid simulations: from ion to fluid scales
  --- reveal kinetic processes

* (3) Laboratory experiments : new, 3rd scientific tool !
  --- in-situ generation of collisionless shocks
  --- initial, boundary conditions controlable (in principle)

Studies of collisionless shocks

Methods	Pros	Cons
Observations of astrophysical objects	・see the whole system. ・see evolved (t→∞). ・less boundary effects.	・difficult to see time evolution. ・worse angular resolution. ・unable to directly measure distribution functions, elemag fields.
“In-situ” observations by satellites	・rich observables (distribution func./elemag fields). ・short cadence	・M~10 : uncontrolable. ・only measurable at satellites.
Simulations	・set initial and boundary conditions. ・see all observables at arbitrary place and epoch.	・huge CPU time in 3D cases ・unrealistic parameters. ・limited spatial and time scales
Laboratory Experiments	・set initial and boundary conditions. ・see all observables at arbitrary place and epoch. ・Real parameters/physical quantities.	・less people joining! ・limited spatial and times scales. ・methods unestablished.

Previous shock experiments

- Many collisional shock generation (many authors)
- Collisionless shocks in unmagnetized plasmas: w/o external B.
  --- Kuramitsu et al. (2011) with GXII: electrostatic shocks.
  --- Sakawa et al. (coming soon?) with NIF: "Weibel" shocks.
- Collisionless shocks in magnetized plasmas: w/ external B.
  --- Paul et al. (1965) via Z-pinch: $M_A < 10$
  --- Niemann et al. (2014) with UCLA/LAPD: $M_A < 2$
  --- Schaeffer et al. (2017) with $M_A \sim 10$

Our advantage over previous works:
* simultaneous measurements of density and temperature across the shock via *collective Thomson scattering*.
* simple setup to have supercritical magnetized shock: $M_A > 3$

Previous shock experiments

- Many collisional shock generation (many authors)
- Collisionless shocks in unmagnetized plasmas: w/o external B.
  --- Kuramitsu et al. (2011) with GXII: electrostatic shocks.
  --- Sakawa et al. (coming soon?) with NIF: “Weibel” shocks.

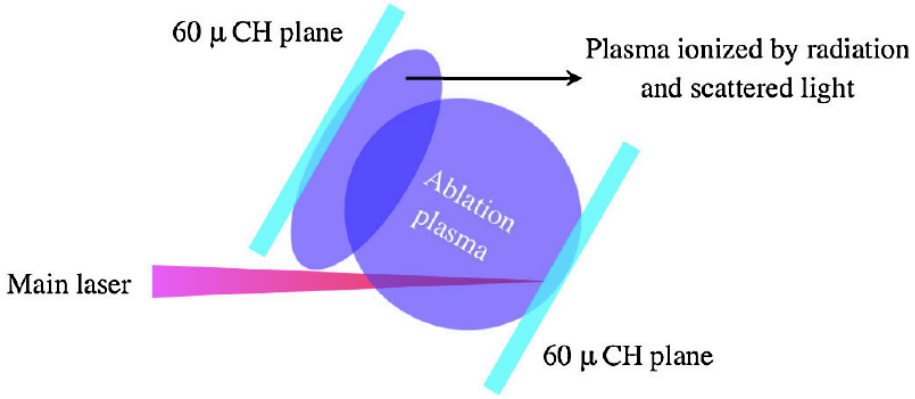

FIG. 1 (color online). Schematic of the double-plane target. The separation between two planes was 4.5 mm. The target normal lies 30° from the laser axis.

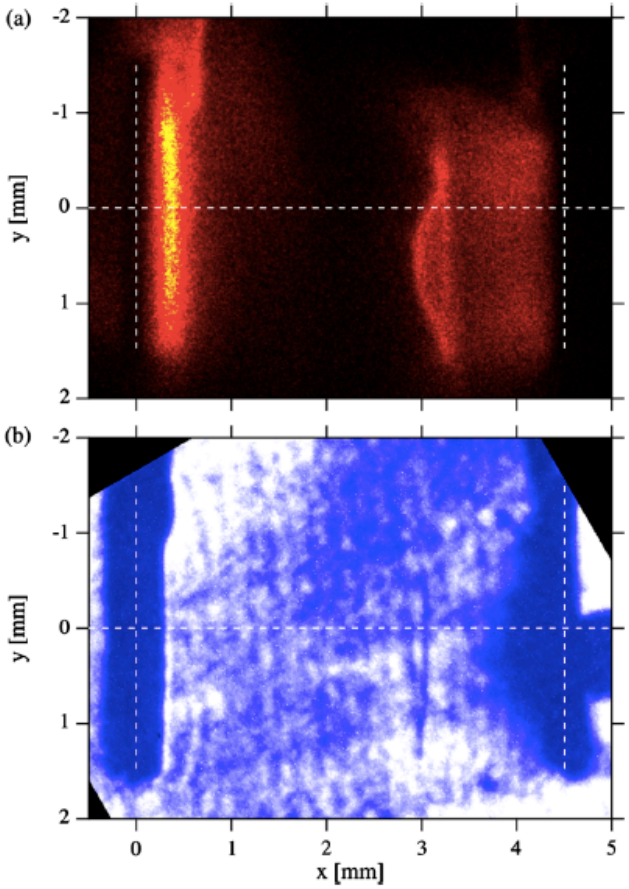

FIG. 4 (color online). (a) Self-emission snapshot at $t = 25$ ns taken on the same shot as Fig. 2. (b) Shadowgraphy snapshot at $t = 25$ ns taken on a different shot.

Kuramitsu et al. (2011), PRL

Previous shock experiments

- Collisionless shocks in magnetized plasmas: w/ external B.

--- Paul et al. (1965) via Z-pinch: M_A <10.

--- Morita et al. (2013) with GekkoXII: M_A~ 1.

--- Niemann et al. (2014) with UCLA/LAPD: M_A< 2.

--- Schaeffer et al. (2017) with OMEGA: M_{ms}~12.

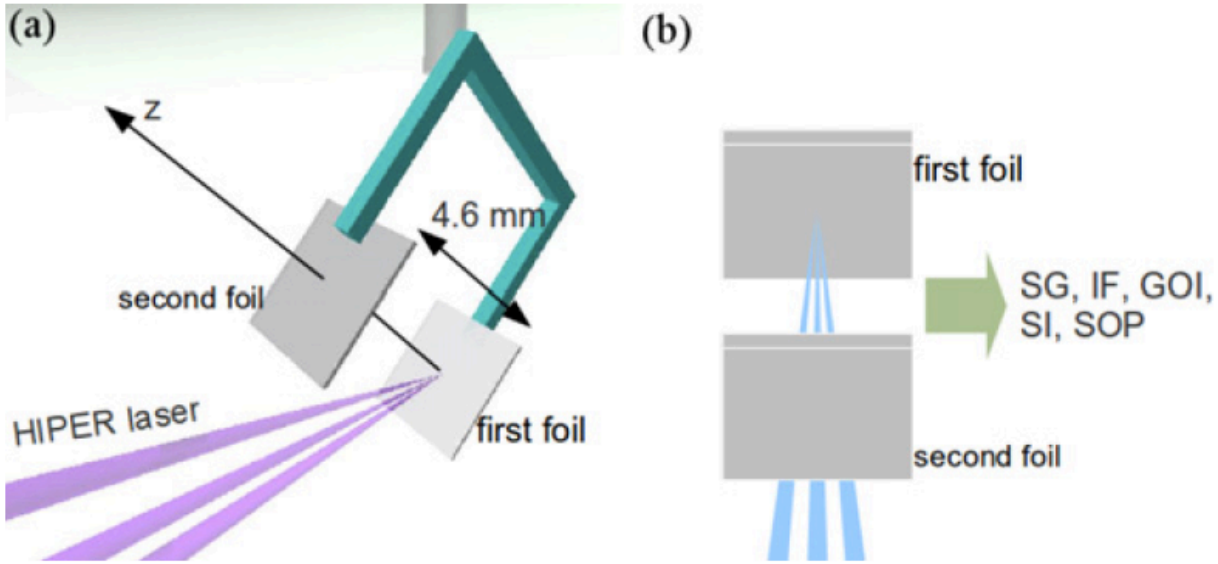

Figure 1. (a) The schematic view of the target. The first foil is irradiated by three beams to produce counter-streaming plasmas between two foils. (b) The top view of the target. The plasmas are diagnosed by the SG, GOI, SI, and SOP from the direction perpendicular to the plasma expansion.

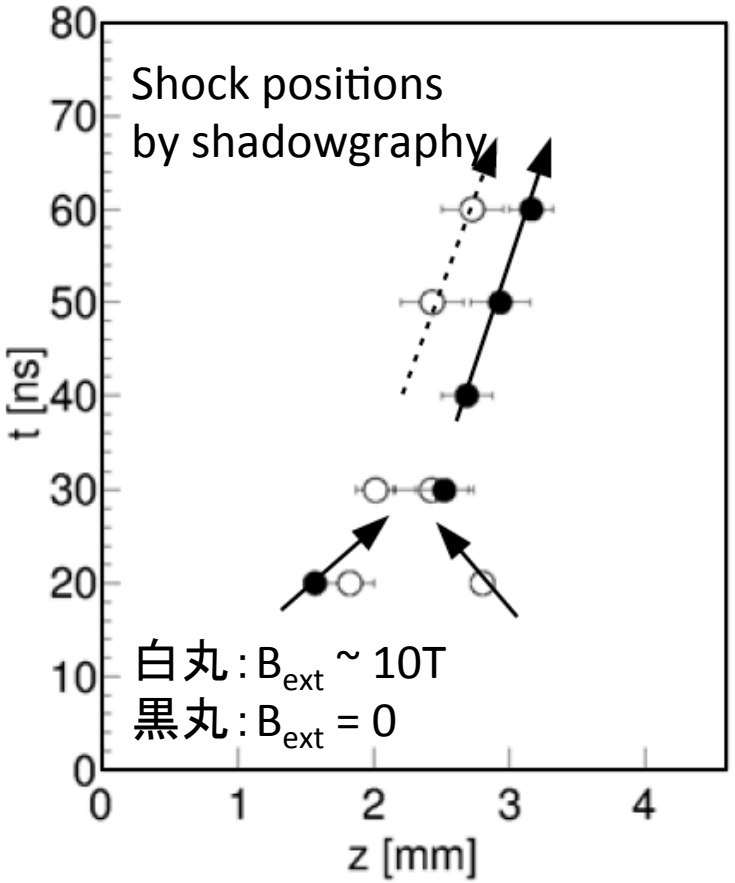

Morita et al. (2013)

Previous shock experiments

- Collisionless shocks in magnetized plasmas: w/ external B.

--- Paul et al. (1965) via Z-pinch: M_A <10.

--- Morita et al. (2013) with GekkoXII: M_A~ 1.

--- Niemann et al. (2014) with UCLA/LAPD: M_A< 2.

--- Schaeffer et al. (2017) with OMEGA: M_{ms}~12.

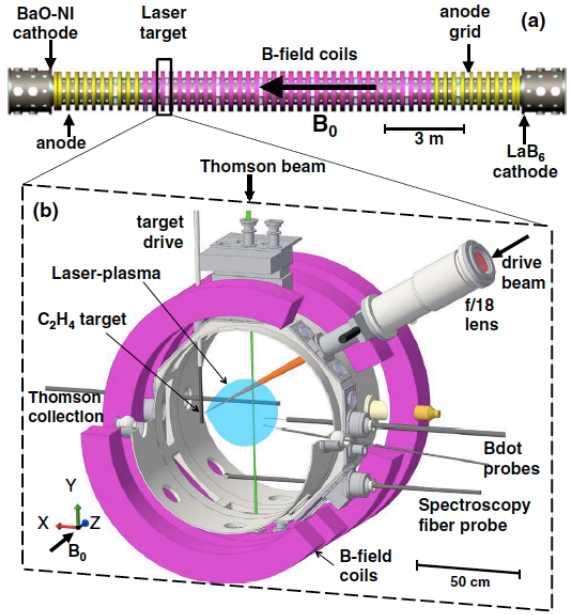

Figure 1. Schematic of (a) the LAPD and (b) the laser-target and diagnostics configuration.

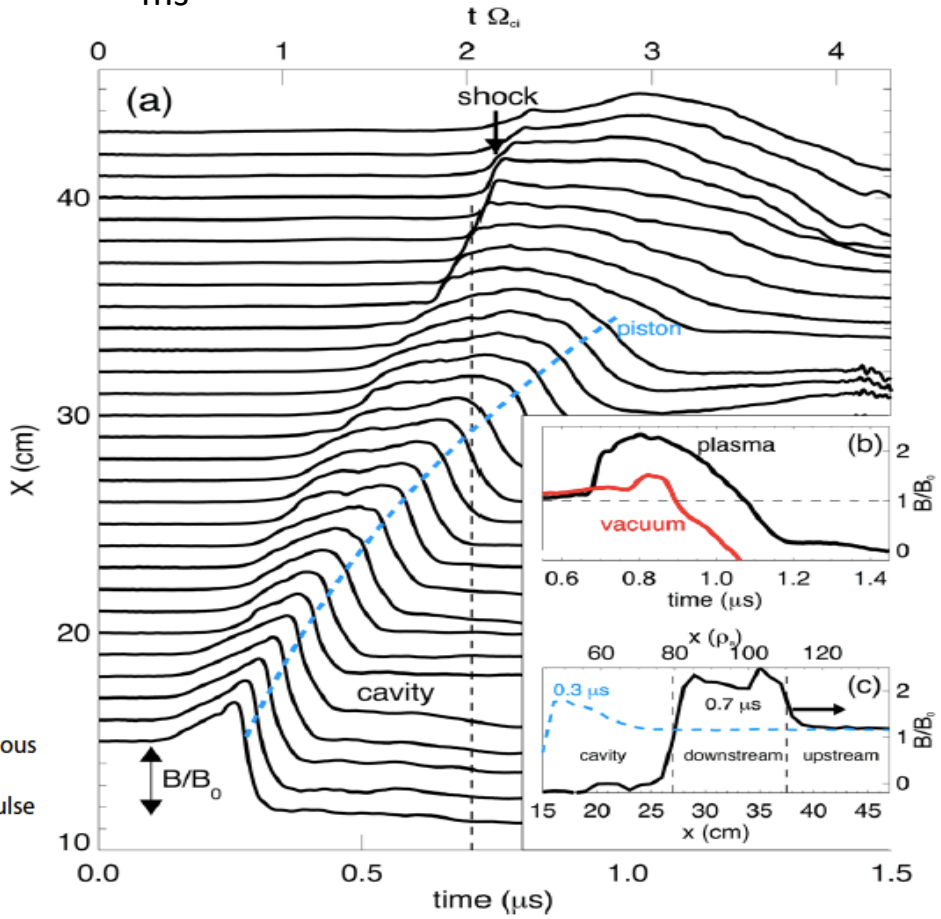

Figure 2. (a) Magnetic stack plots of B_z as a function of time for various distances from the target. (b) Comparison of B_z(t) at x = 35 cm with (black) and without (red) the ambient plasma. (c) Structure of the pulse before (t = 0.3 μs) and after a shock is formed (t = 0.7 μs).

Niemann et al. (2014), GRL

Previous shock experiments

- Collisionless shocks in magnetized plasmas: w/ external B.

--- Paul et al. (1965) via Z-pinch: M_A <10.

--- Morita et al. (2013) with GekkoXII: M_A~ 1.

--- Niemann et al. (2014) with UCLA/LAPD: M_A< 2.

--- Schaeffer et al. (2017) with OMEGA: M_{ms}~12.

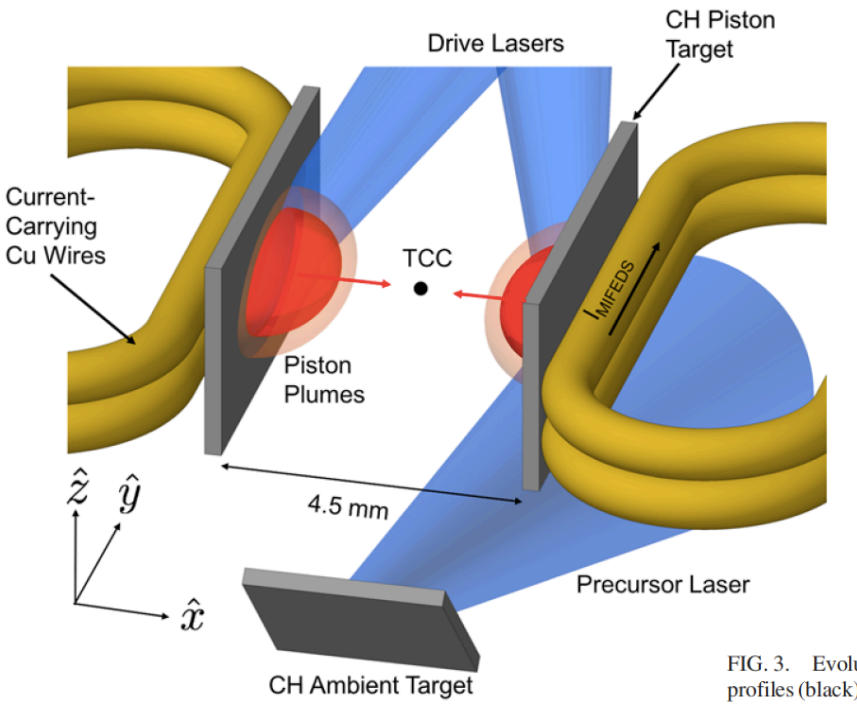

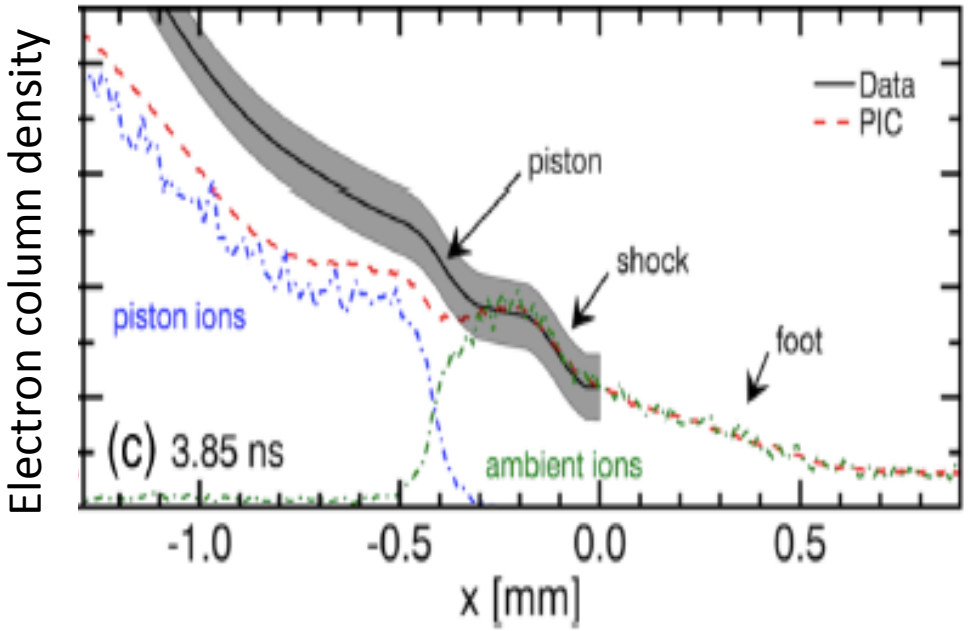

Schaeffer et al. (2017), PRL

FIG. 3. Evolution of line-integrated electron density profiles at (a) 2.35, (b) 2.85, and (c) 3.85 ns after laser ablation. For each, the density profiles (black) were reconstructed by linearly interpolating between the gradient density values associated with each AFR band edge and, in the regions of the density jumps, utilizing the shadowgraphy profiles. The constant density offset was estimated from simulations, and the shaded band corresponds to the uncertainty in this offset. Also shown are the corresponding profiles from PSC PIC simulations (red). Additionally, in (c) the ambient (green) and piston (blue) contributions to the total electron density in the PIC simulations are shown. [(a), inset] Raw shadowgraphy signal (black) and reconstructed relative density (green) profile at 2.35 ns. [(b), inset] Direct comparison of the raw AFR signal (black) and corresponding synthetic simulation signal (red) at 2.85 ns. For both, the signals have been reduced to binary for simplicity. In all plots, the plasma moves toward $x = 0$.

Experimental setup

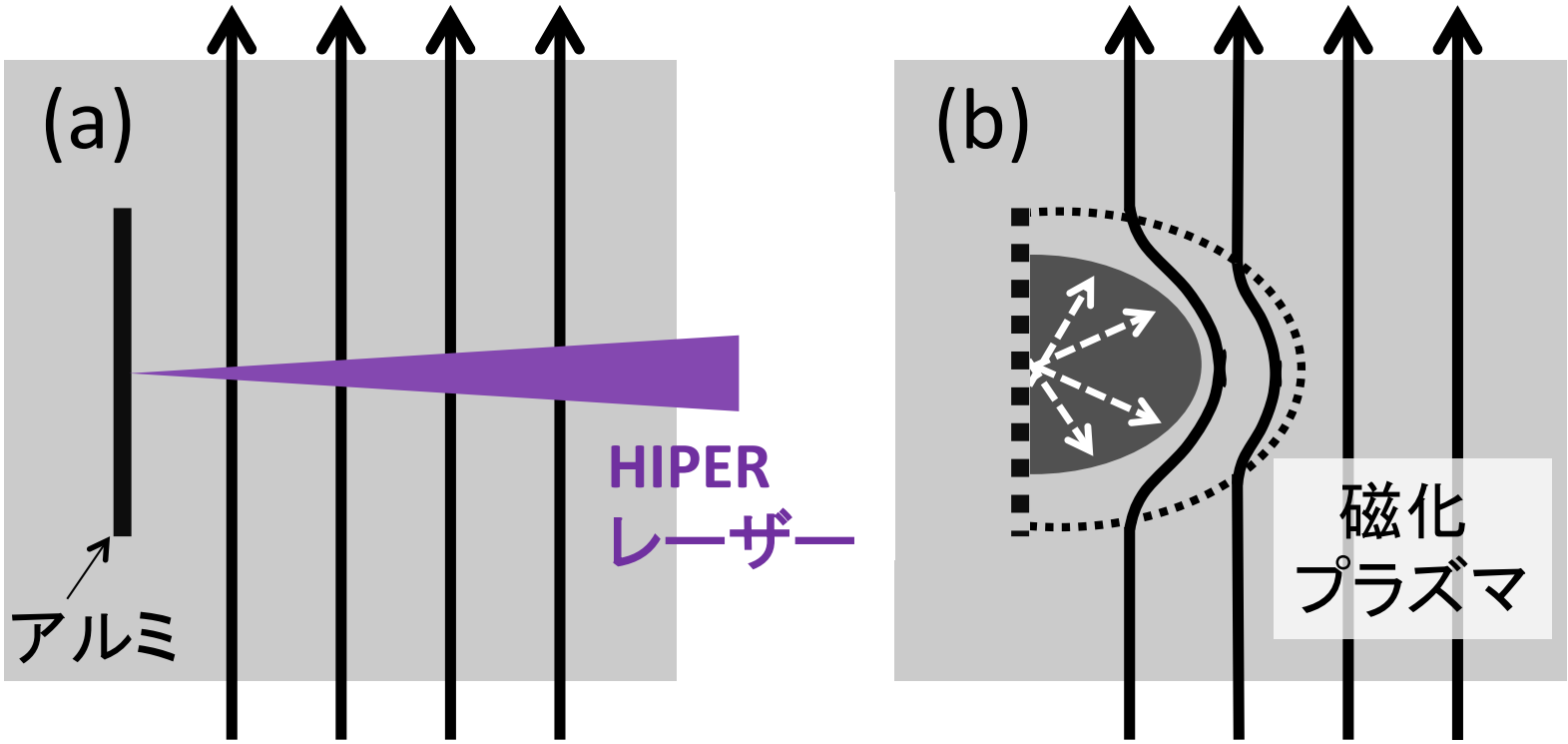

(a) 雰囲気ガス中に外部磁場（黒矢印）をかけた状態でHIPERレーザーを照射する。

(b) ショット後、アルミ薄膜由来のプラズマ(白矢印の様に膨張)とアルミからの輻射で電離して生成された磁化プラズマの相互作用によってmagnetized shock (黒点線)ができる。

Experimental setup

GXII HIPER lasers : 700 J/beam x 4, 1ω (1053nm), 1.3ns width, 1.4~2 mm spots
Ambient gas : N_2 (5 torr)
Target: Al (2 mm thickness)
Helmholtz coils provide B~1.6 T at the target chamber center.

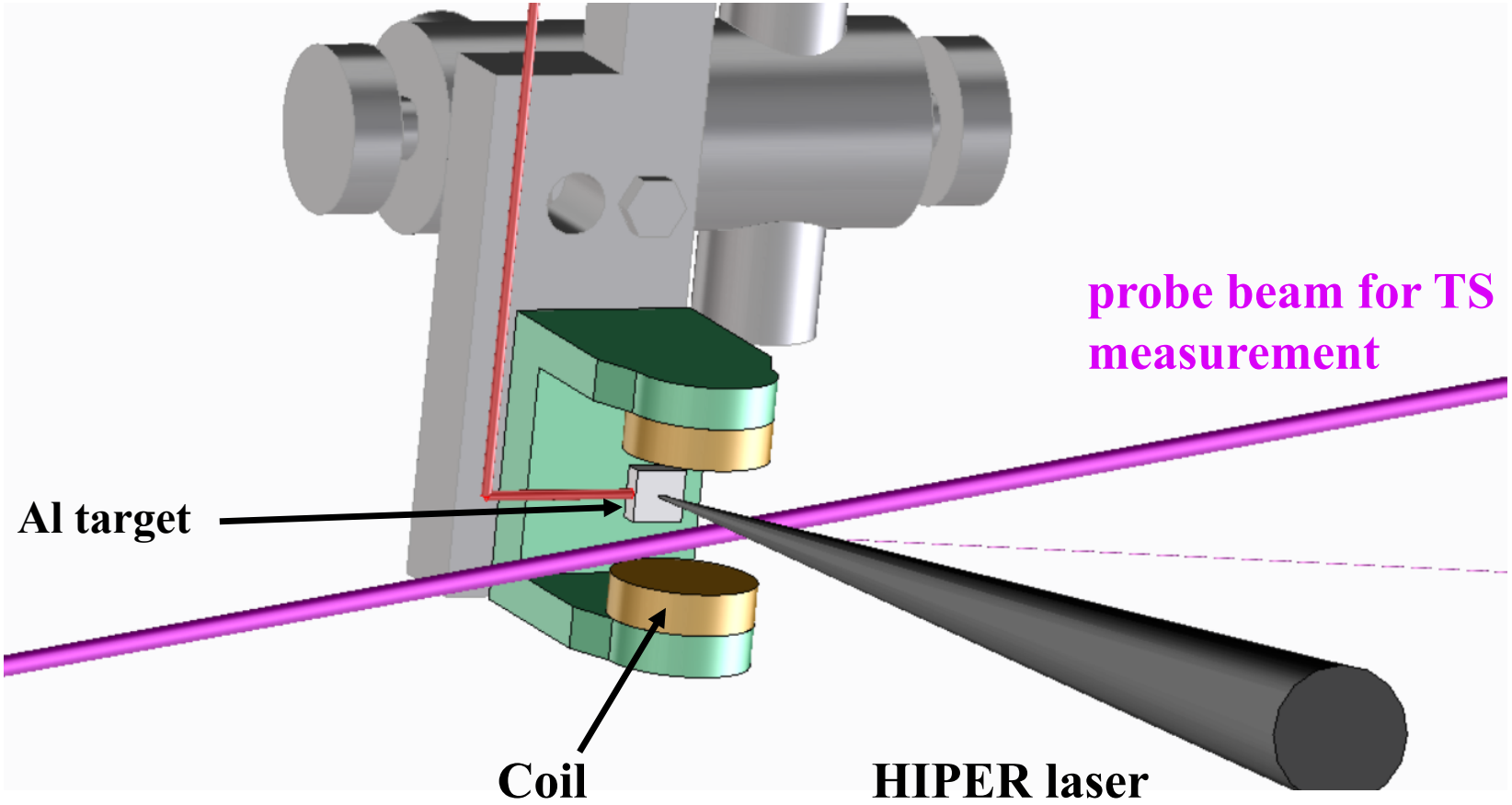

Shock dynamics

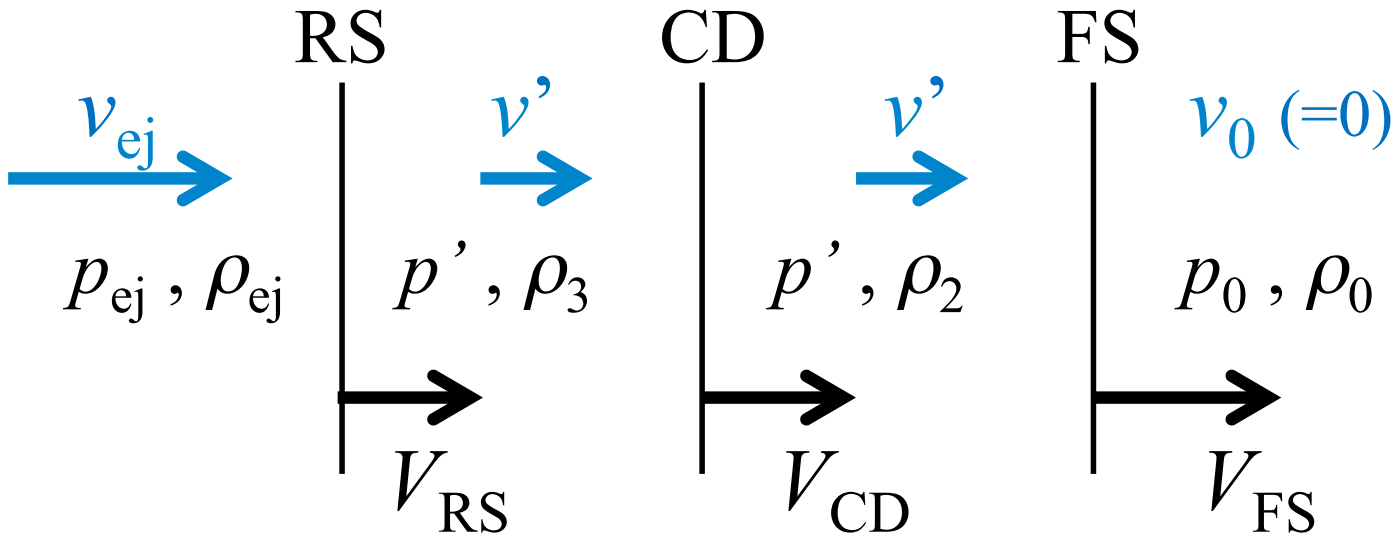

圧縮比： $\alpha = \dfrac{\rho_2}{\rho_0} = \dfrac{-V_{\rm FS}}{v_2 - V_{\rm FS}}$ $\beta =, \dfrac{\rho_3}{\rho_{\rm ej}} = \dfrac{v_{\rm ej} - V_{\rm RS}}{v' - V_{\rm RS}}$

$k = \left(\dfrac{\gamma_{\rm ej}+1}{\gamma_0+1} \dfrac{\rho_0}{\rho_{\rm ej}} \right)^{1/2} << 1$ のとき、

$$V_{\rm FS} \approx \frac{\alpha}{\alpha - 1} v_{\rm ej} \ , \qquad V_{\rm RS} \approx v_{\rm ej} \ , \qquad \frac{\Delta R}{R} = \frac{V_{\rm FS} - V_{\rm RS}}{V_{\rm FS}} \approx \frac{1}{\alpha}$$

Biermann 効果が効く！

Biermann battery

From Wikipedia, the free encyclopedia

In astrophysics, the **Biermann battery** is a process by which a weak seed magnetic field can be generated from zero initial conditions.[1] The relative motion between electrons and ions is driven by rotation. The process was discovered by Ludwig Biermann in 1950.[2][3]

A simple derivation of the effect starts with the momentum equation for the free electron fluid, keeping only the electric field and pressure force:

$$m_e \frac{d\vec{v}_e}{dt} = -e\vec{E} - \frac{\nabla p_e}{n_e}.$$

For phenomena on sufficiently slow time scales, the left-hand side of the above equation can be neglected that leads to the Ohm's law for the electric field:

$$\vec{E} = -\frac{\nabla p_e}{e n_e}.$$

The other terms in the general Ohm's law are neglected here since they typically vanish for zero magnetic field and do not spontaneously generate field. Inserting the above electric field into the Faraday's law gives an equation for the magnetic field:

$$\frac{\partial \vec{B}}{\partial t} = \frac{1}{e n_e} \nabla T_e \times \nabla n_e$$

This shows that magnetic fields develop "spontaneously", that is, from initially being zero, when there are non-parallel gradients in electron temperature and density.

Gregori et al. 12, Nature; Kugland et al. 12, Nature Phys.:
アブレーション・プラズマ（＝ピストン・プラズマ、ejecta）は
Biermann効果により磁化する。

$$\nabla T_{\mathrm{e}} \propto -\hat{r} \ , \ \nabla n_{\mathrm{e}} \propto -\hat{z}$$

$$\Rightarrow \frac{\partial \vec{B}}{\partial t} \propto (\nabla T_{\mathrm{e}} \times \nabla n_{\mathrm{e}}) \propto -\hat{\phi}$$

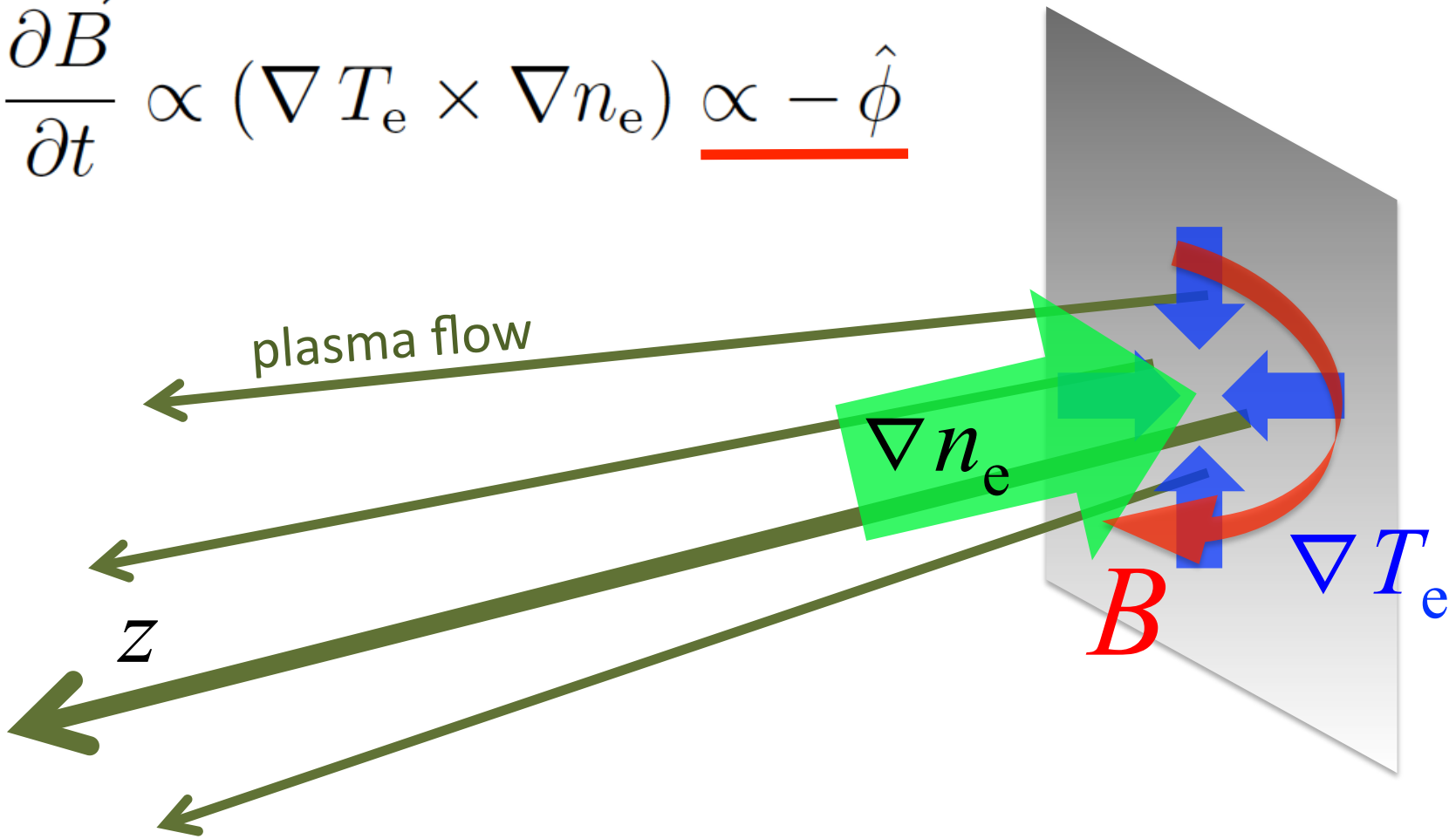

Gregori et al. 12, Nature; Kugland et al. 12, Nature Phys.:
アブレーション・プラズマ（＝ピストン・プラズマ、ejecta）は
Biermann効果により磁化する。

$$\nabla T_{\rm e} \propto -\hat{r} \ , \ \nabla n_{\rm e} \propto -\hat{z}$$

$$\Rightarrow \ \frac{\partial \vec{B}}{\partial t} \propto (\nabla T_{\rm e} \times \nabla n_{\rm e}) \propto -\hat{\phi}$$

$$\Rightarrow \ B \approx \frac{T_e}{eV_d\phi}$$

$$\sim 10\ {\rm T} \left(\frac{T_e}{10^3\ {\rm eV}}\right) \left(\frac{V_d}{10^2\ {\rm km/s}}\right)^{-1} \left(\frac{\phi_{\rm f}}{1\ {\rm mm}}\right)^{-1}$$

($T_{\rm e}$: 電子温度, $V_{\rm d}$: flow速度, $\phi_{\rm f}$: focal spot size)

MHD shock tube
窒素に外部磁場あり(1.5T)の場合

	１:アルミプラズマ	２:窒素プラズマ
質量密度:	rho1 = 1.88 x 10^{-4} g/cc	rho2 = 1.17 x 10^{-5} g/cc
温度:	T1 = 10 eV	T2 = 30 eV
磁場強度:	B1 = 10 T	B2 = 1.5 T
速度:	v1 = 500 km/s	v2 = 0 km/s

CANSを用いて計算

窒素中の衝撃波: $M_A = 34, M_s = 22$

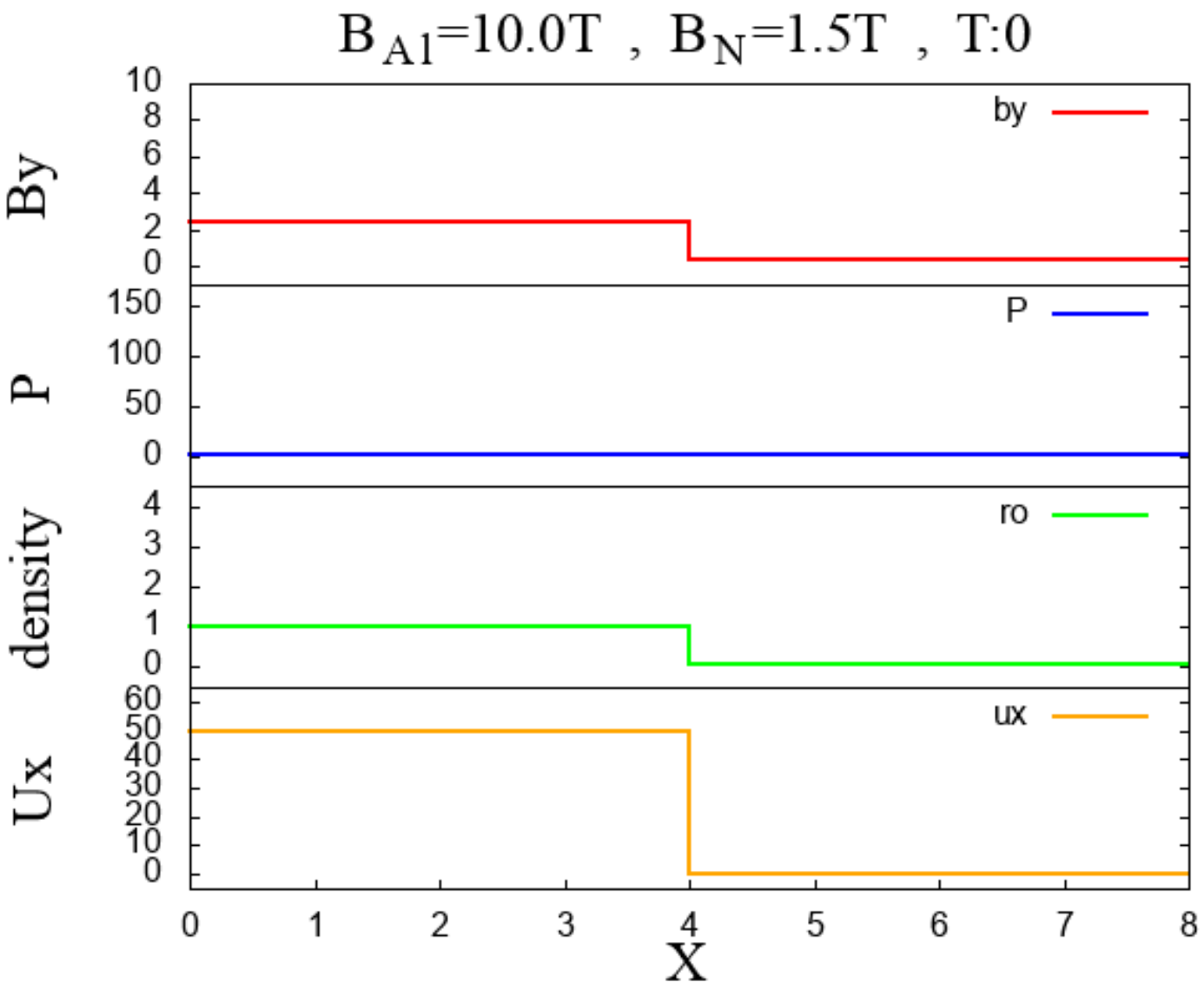

MHD shock tube
窒素に外部磁場あり(0.5T)の場合

	１:アルミプラズマ	２:窒素プラズマ
質量密度:	rho1 = 1.88 x 10^{-4} g/cc	rho2 = 1.17 x 10^{-5} g/cc
温度:	T1 = 10 eV	T2 = 30 eV
磁場強度:	B1 = 10 T	B2 = 0.5 T
速度:	v1 = 500 km/s	v2 = 0 km/s

CANSを用いて計算

窒素中の衝撃波: $M_A = 98, M_s = 21$

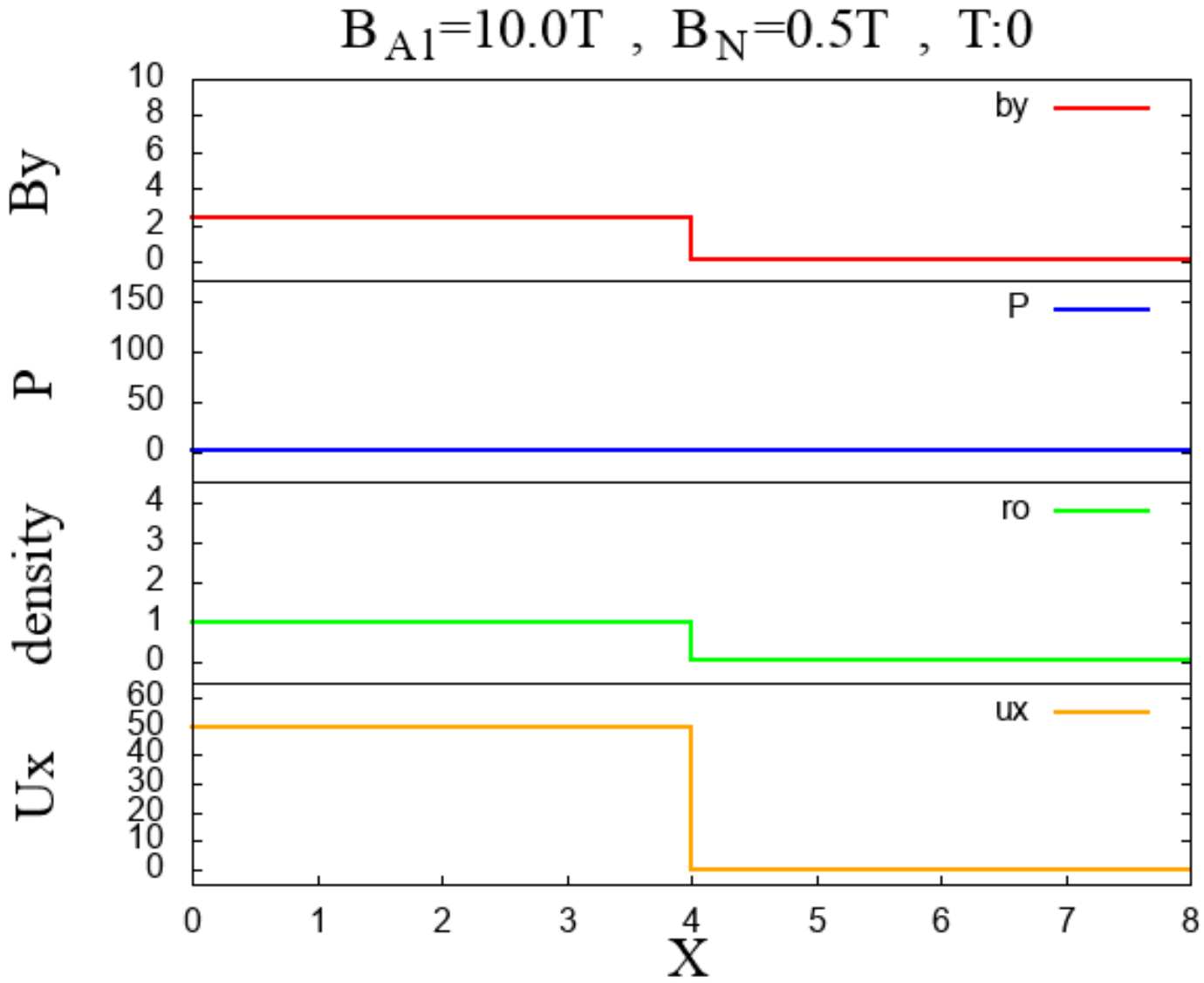

MHD shock tube
窒素に外部磁場なしの場合

	１：アルミプラズマ	２：窒素プラズマ
質量密度：	rho1 = 1.88 x 10^{-4} g/cc	rho2 = 1.17 x 10^{-5} g/cc
温度：	T1 = 10 eV	T2 = 30 eV
磁場強度：	B1 = 10 T	B2 = 0 T
速度：	v1 = 500 km/s	v2 = 0 km/s

CANSを用いて計算

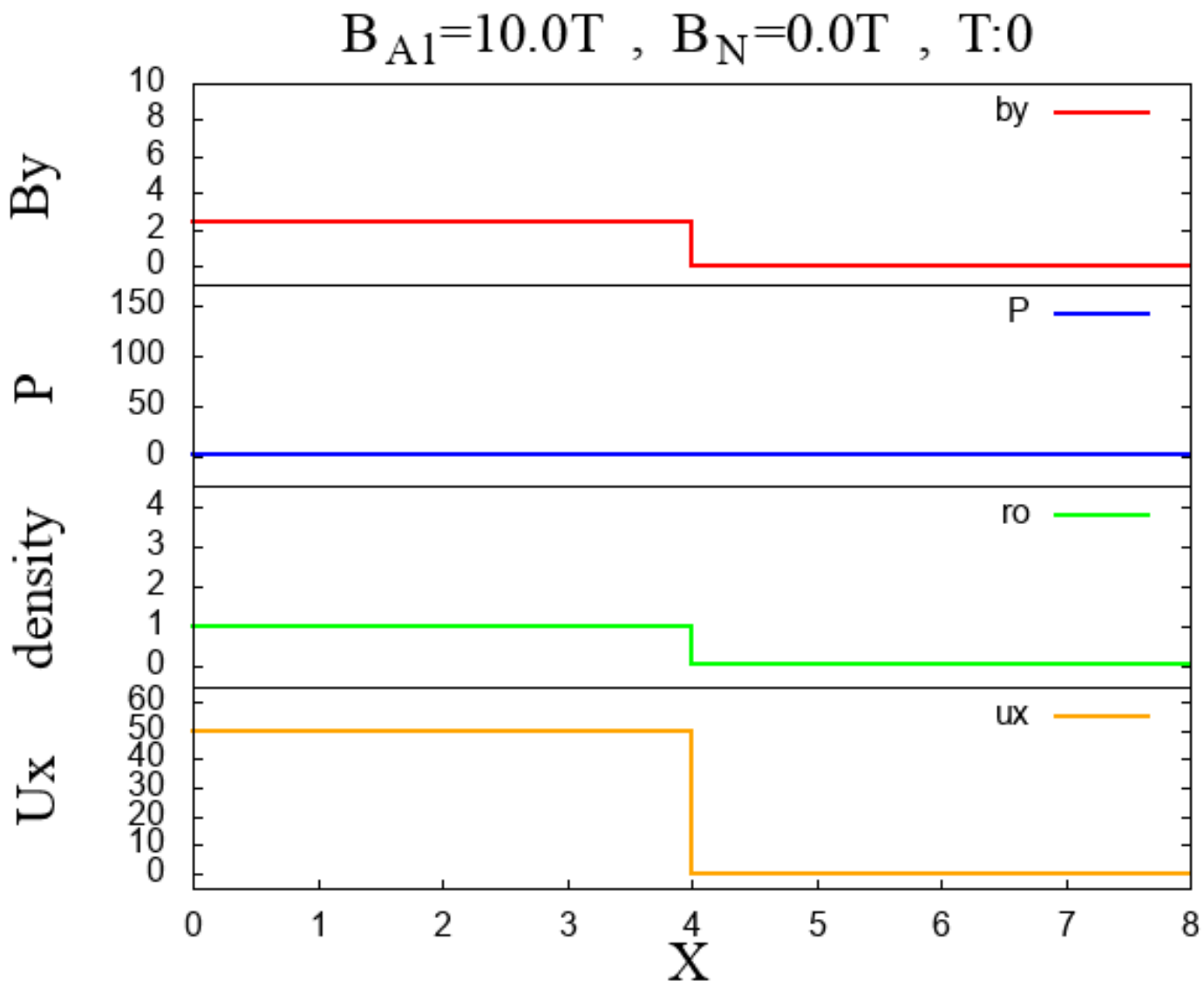
B Al=10.0T , B N=0.0T , T:0
By
P
density
Ux
by
P
ro
ux
X
10
8
6
4
2
0
150
100
50
0
4
3
2
1
0
60
50
40
30
20
10
0
0
1
2
3
4
5
6
7
8

1D PIC simulations

Quantity	Aluminum plasma	Nitrogen plasma
Drift velocity V_d [km/s]	500	0
Magnetic field B_0 [T]		
Run 1	10.0	0.5
Run 2	10.0	0.0
Run 3	0	0.5
Run 4	0	0.0
Electrons		
Density N_e [cm^{-3}]	3.75×10^{19}	1.5×10^{18}
Plasma frequency f_{pe} [Hz]	5.51×10^{13} / 5.51×10^{12}	1.1×10^{13} / 1.1×10^{12}
Temperature T_e [eV]	10	30
Thermal velocity V_{te} [km/s]	1,330	2,300
Debye length λ_{De} [m]	3.71×10^{-9} / 3.71×10^{-8}	3.32×10^{-8} / 3.32×10^{-7}
Inertial length d_e [m]	8.39×10^{-7}	4.33×10^{-6}
Cyclotron frequency f_{ce} [Hz]	2.8×10^{11}	1.4×10^{10}
Thermal gyro radius r_e [m]	7.55×10^{-7}	2.62×10^{-5}
Plasma beta	1.62	72.99
Ions		
Charge number Z	9	3
Mass ratio m_i/m_e	49572	25704
Density N_i [cm^{-3}]	4.17×10^{18}	5.0×10^{17}
Plasma frequency f_{pi} [Hz]	7.43×10^{11} / 7.43×10^{10}	1.19×10^{11} / 1.19×10^{10}
Temperature T_e [eV]	10	30
Thermal velocity V_{ti} [km/s]	5.97	14.3
Debye length λ_{Di} [m]	3.71×10^{-9} / 3.71×10^{-8}	3.32×10^{-8} / 3.32×10^{-7}
Inertial length d_i [m]	6.23×10^{-5}	4.01×10^{-4}
Cyclotron frequency f_{ci} [Hz]	5.08×10^{7}	1.63×10^{6}
Thermal gyro radius r_i [m]	1.87×10^{-5}	1.4×10^{-3}
Alfvén velocity V_A [km/s]	19.99	4.11
Plasma beta	0.18	24.33
Grid spacing Δx [m]	8.3×10^{-8}	
Time step Δt [sec]	2.6×10^{-15}	
Number of grids N_x	120,000	
Number of steps N_t	6,000,000	
Speed of light c [km/s]	300,000 / 30,000	
	(laboratory) / (numerical)	

アルミ(ピストン)プラズマが磁化している場合: B(Al) = 10 T

B(窒素) = 0

B(窒素) = 0.5 T

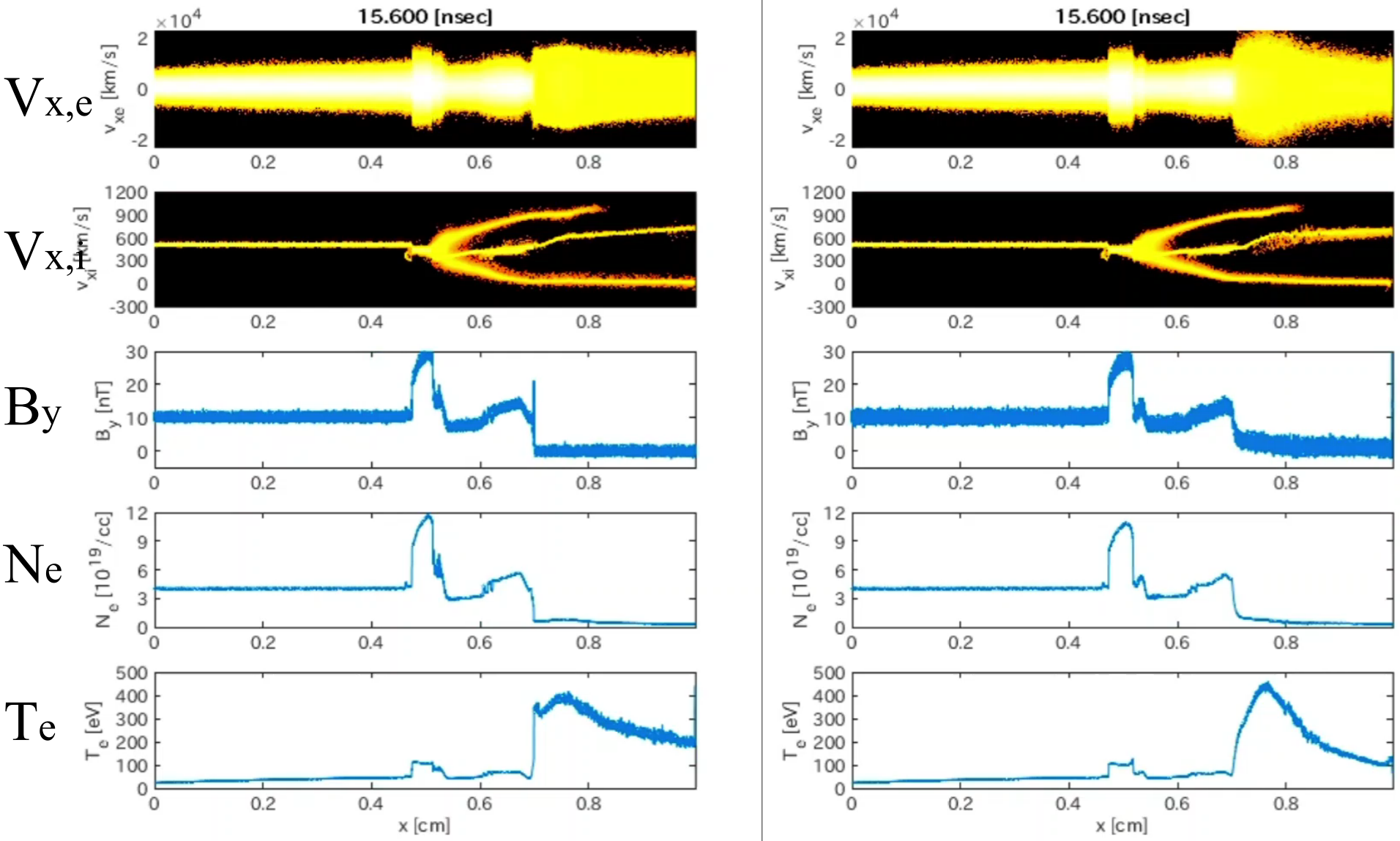

Umeda, RY, et al. submitted

アルミ(ピストン)プラズマが磁化している場合: B(Al) = 10 T

B(窒素) = 0

B(窒素) = 0.5 T

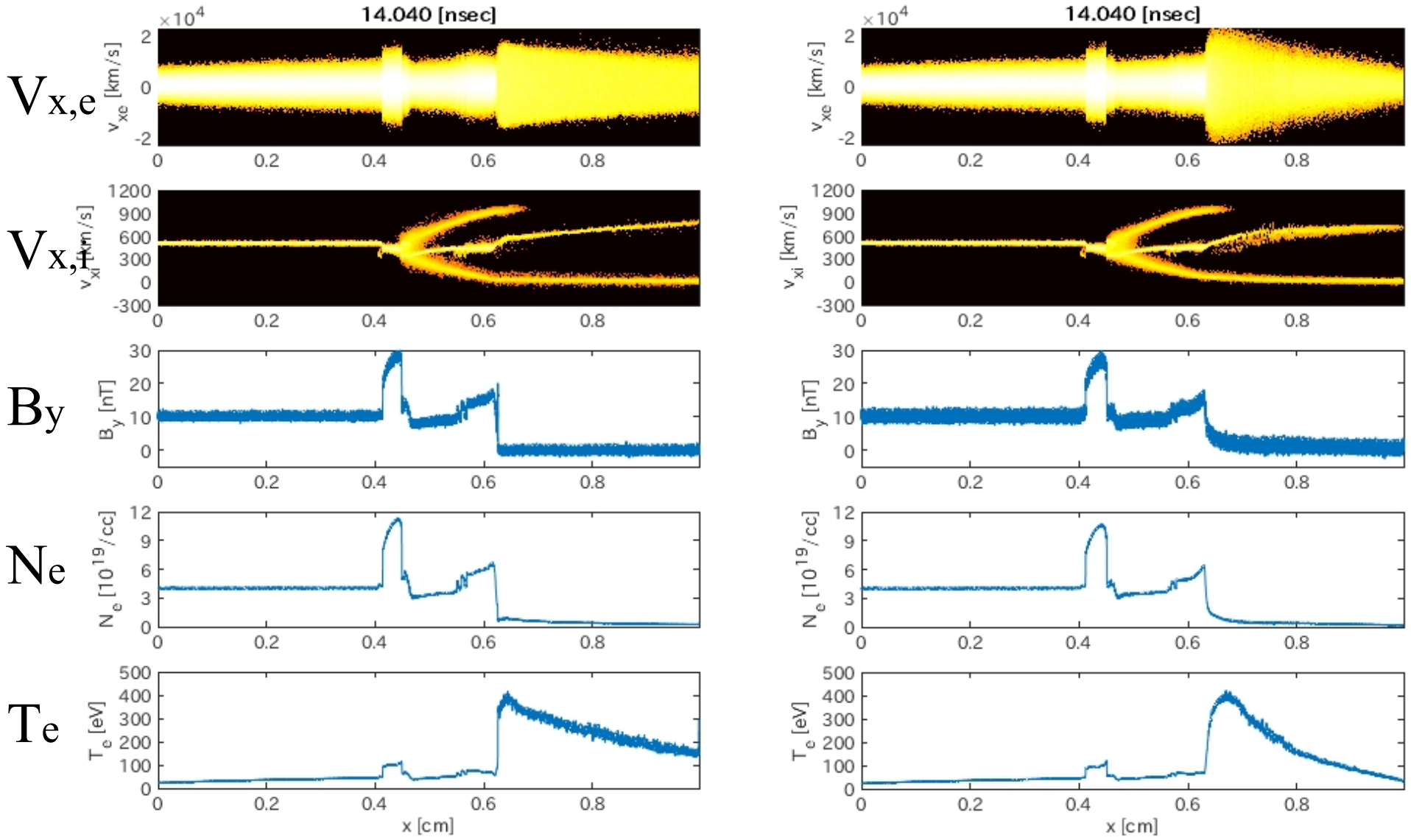

Umeda, RY, et al. submitted

アルミ(ピストン)プラズマが磁化していない場合: B(Al) = 0 T

B(窒素) = 0

B(窒素) = 0.5 T

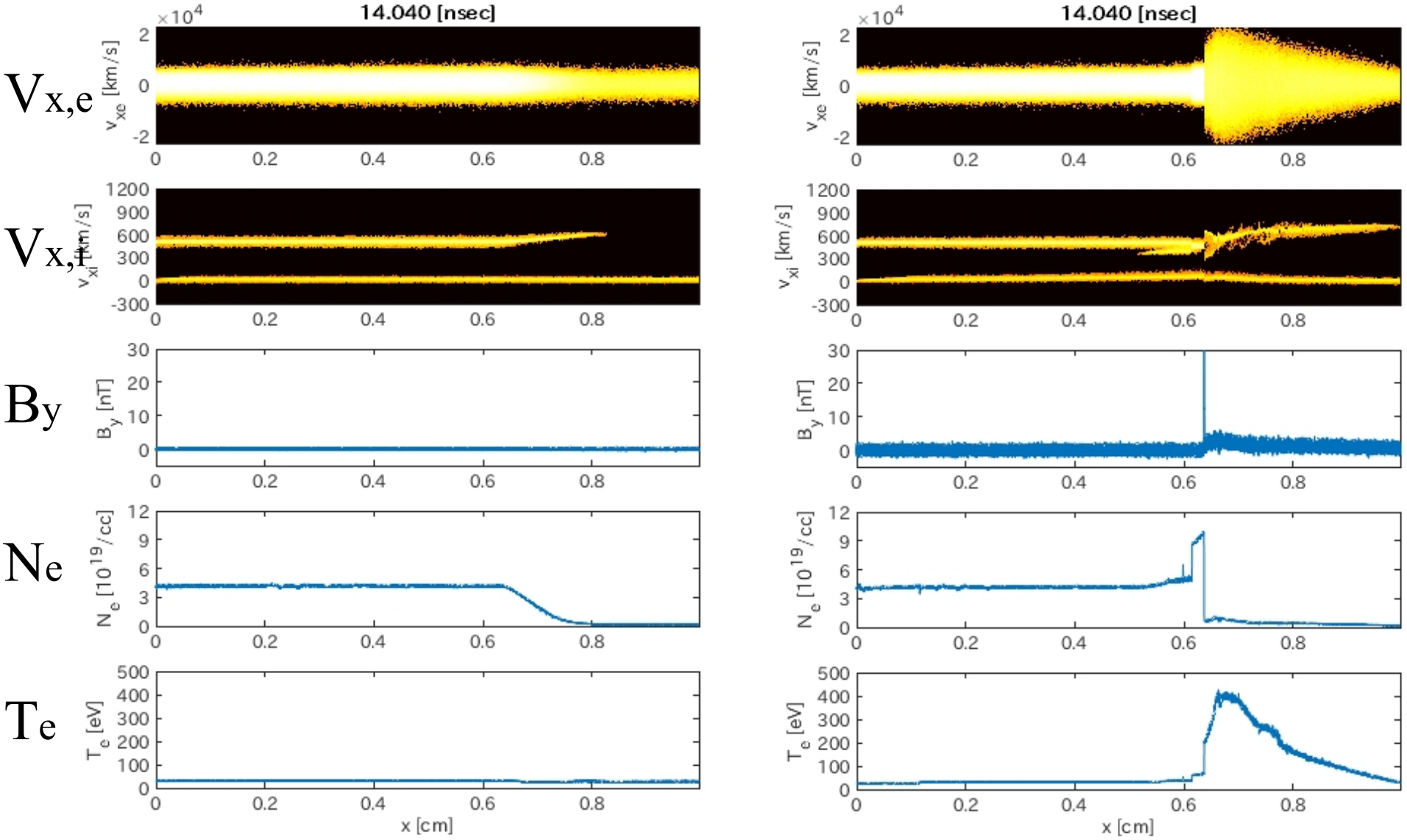

Umeda, RY, et al. submitted

アルミ(ピストン)プラズマが磁化している場合: B(Al) = 10 T

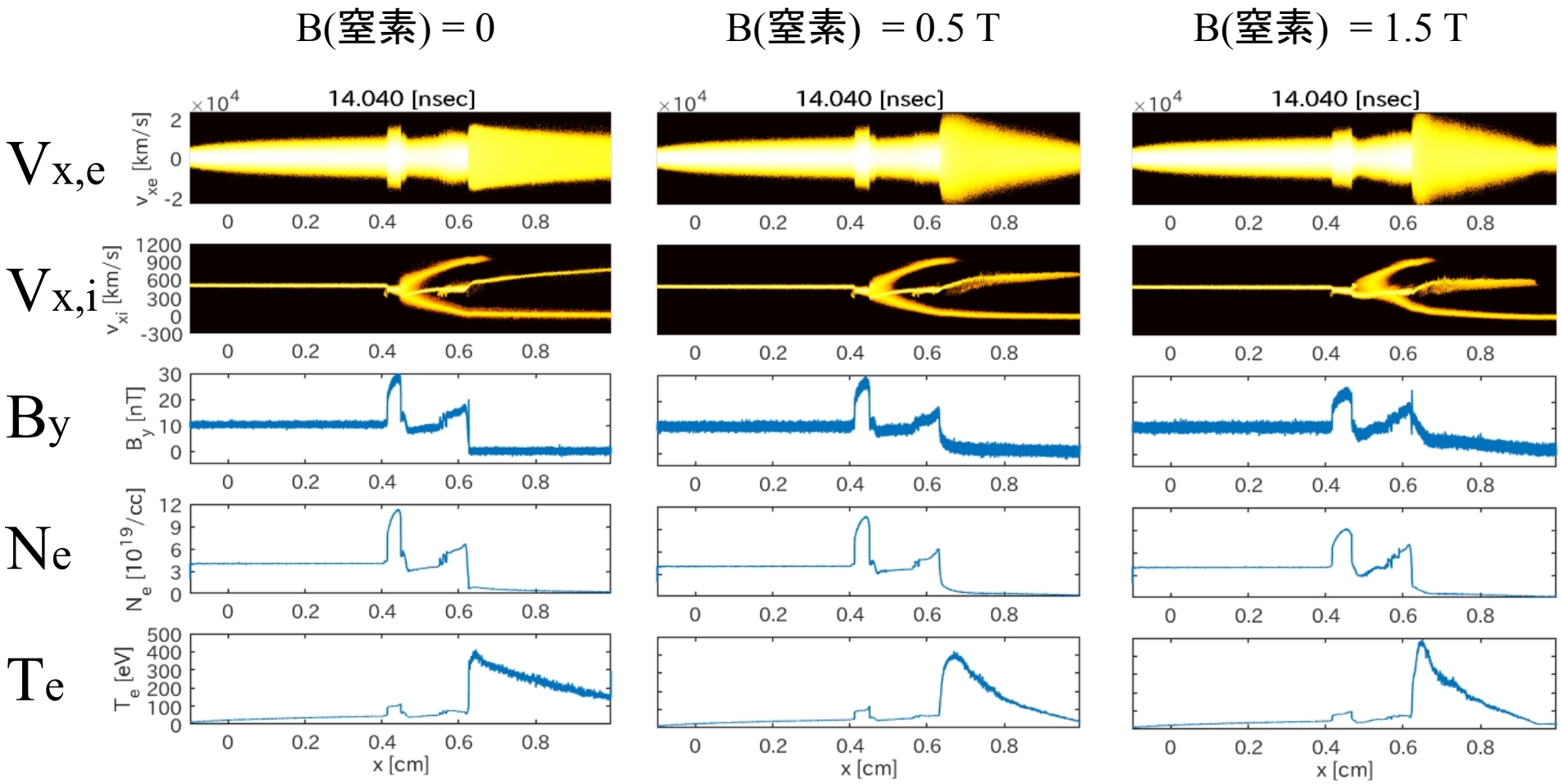

Umeda, RY, et al. submitted; Umeda, RY et al. in prep.

アルミ(ピストン)プラズマが磁化している場合: B(Al) = 10 T

B(窒素) = 3T

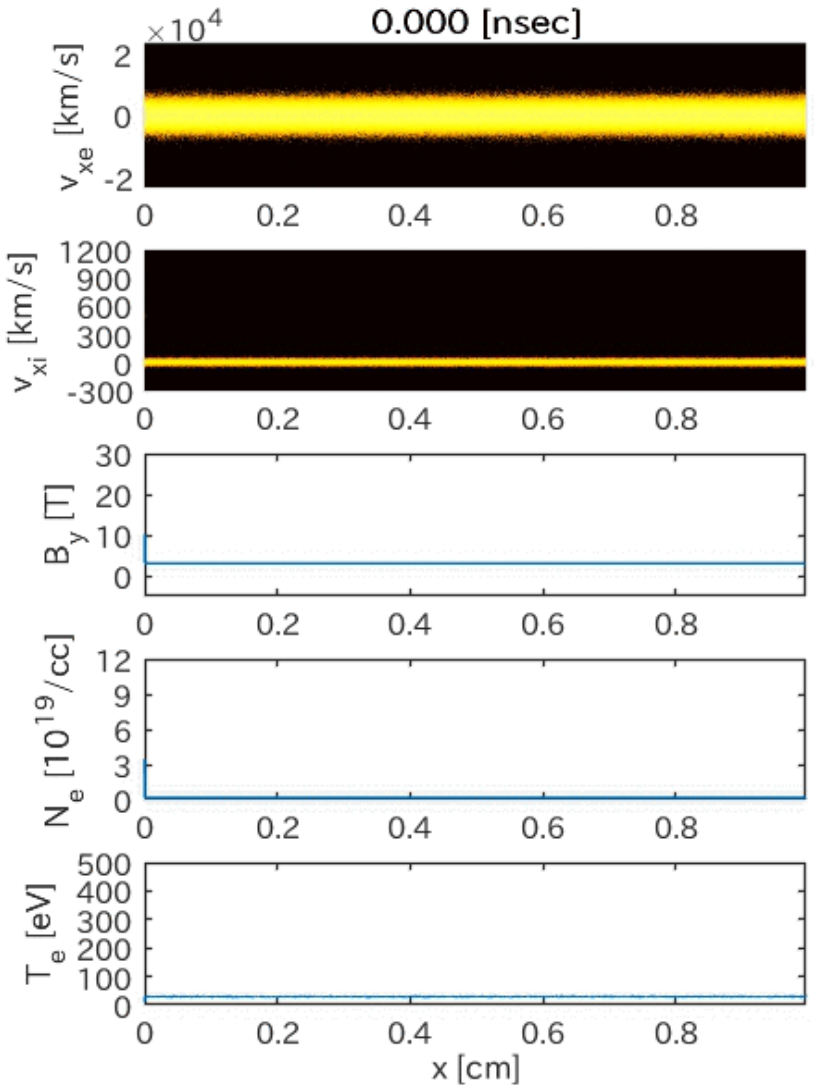

B(窒素) = 5 T

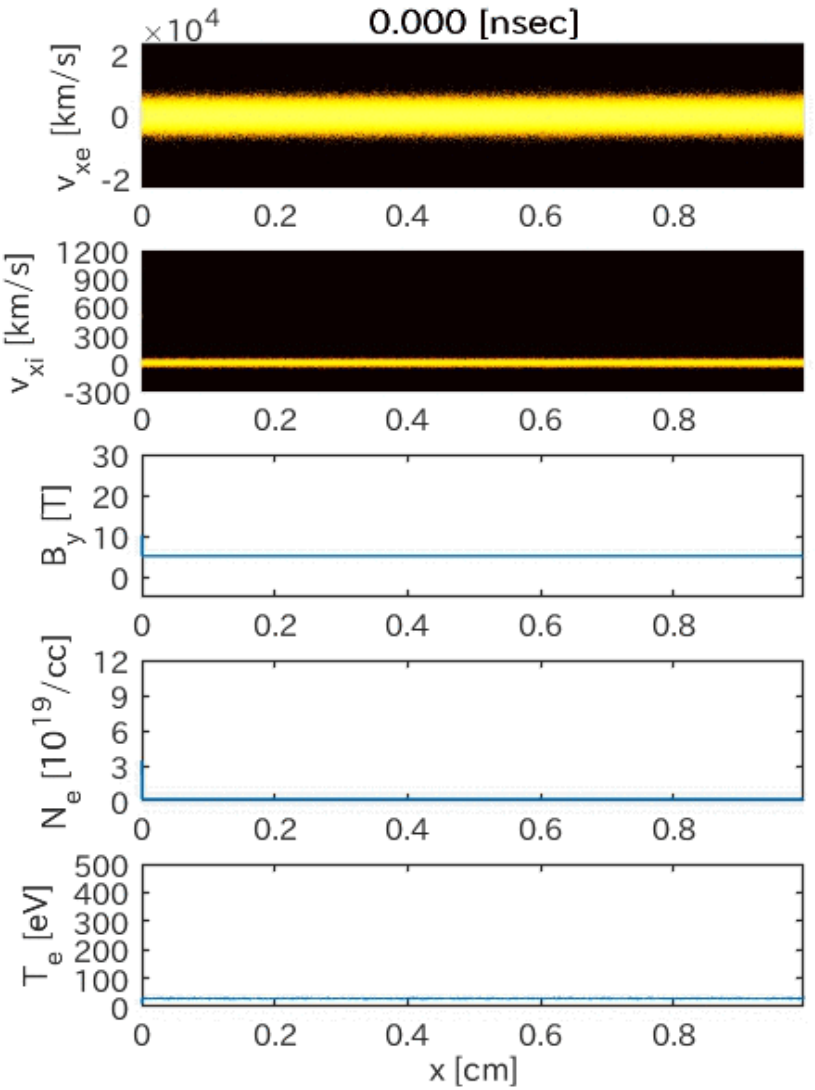

Spatial profile of $n_e/T_e^{1/2}$ at 14 ns after shot

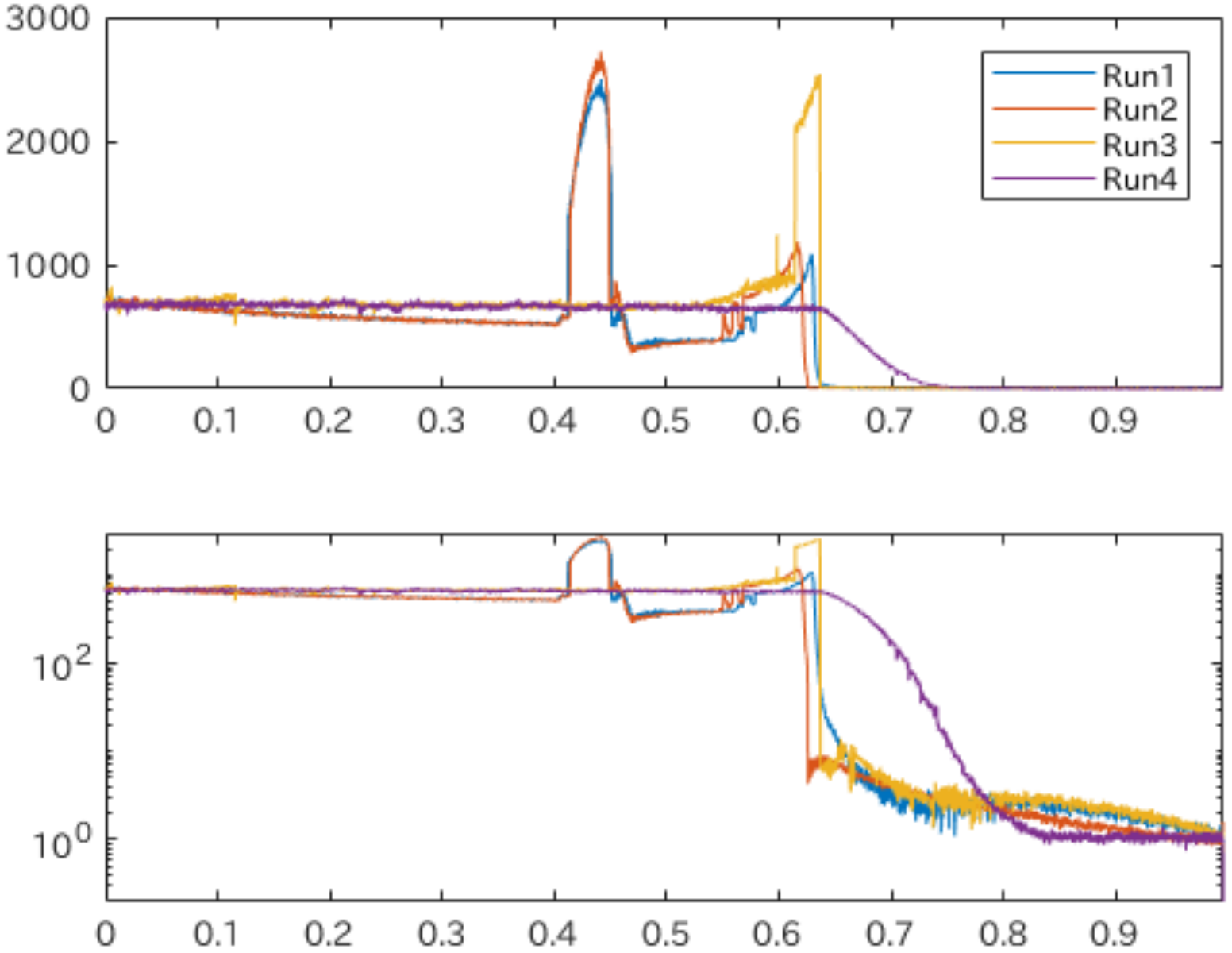

Run 1:
B_{Al} = 10 T
B_N = 0.5 T

Run 1:
B_{Al} = 10 T
B_N = 0 T

Run 1:
B_{Al} = 0 T
B_N = 0.5 T

Run 1:
B_{Al} = 0 T
B_N = 0 T

外部磁場印加装置

・青学で設計、九州大・北九州高専で製作。
コイル: 内径=20mm, 外径=30mm, 巻き数20
コイル間距離: 20mm (ホルダ間距離=15mm)
コンデンサ: 3000μF × 4個 (最大電圧800V)。
印加磁場: 電圧400Vで充電。
ショットの瞬間に放電(~5万アンペア)。
B~1.6 T, duration~100 μs

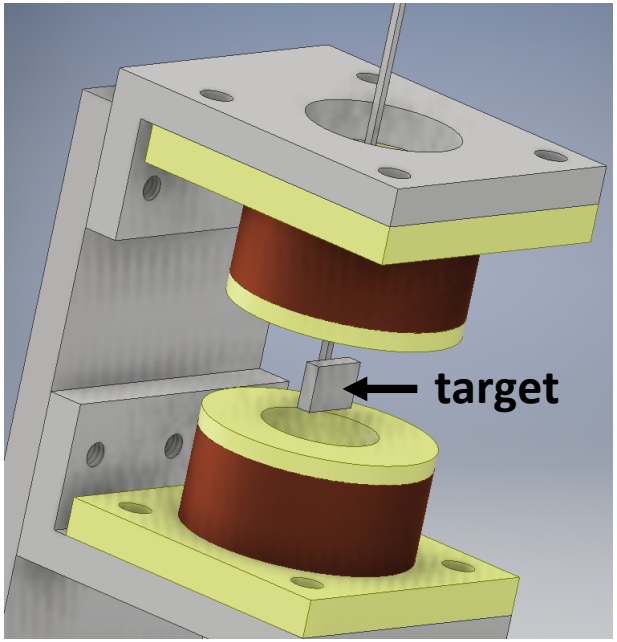

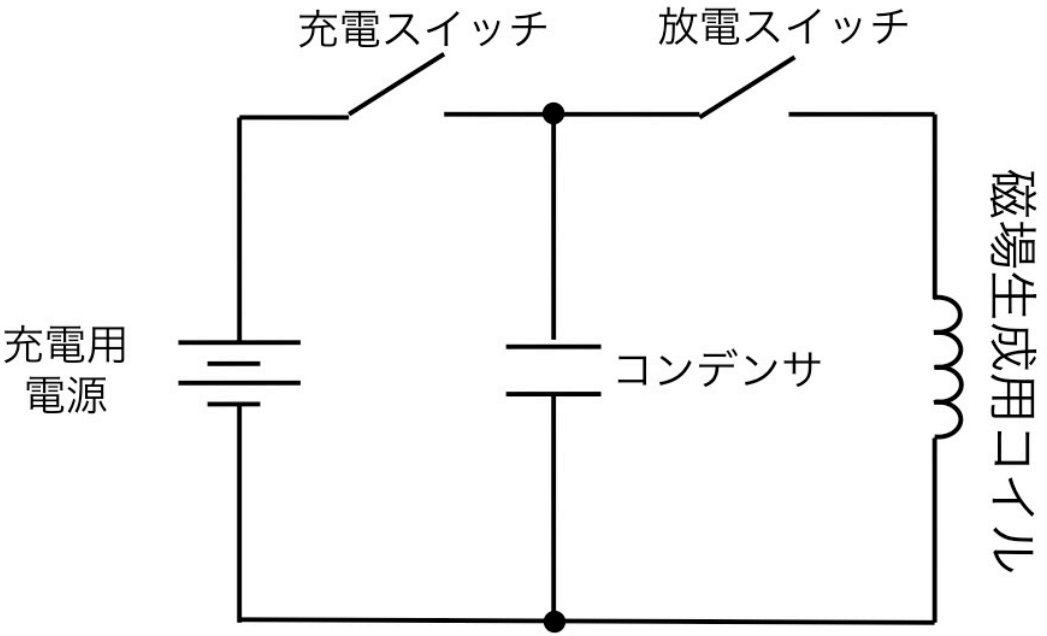

(森田太智氏)

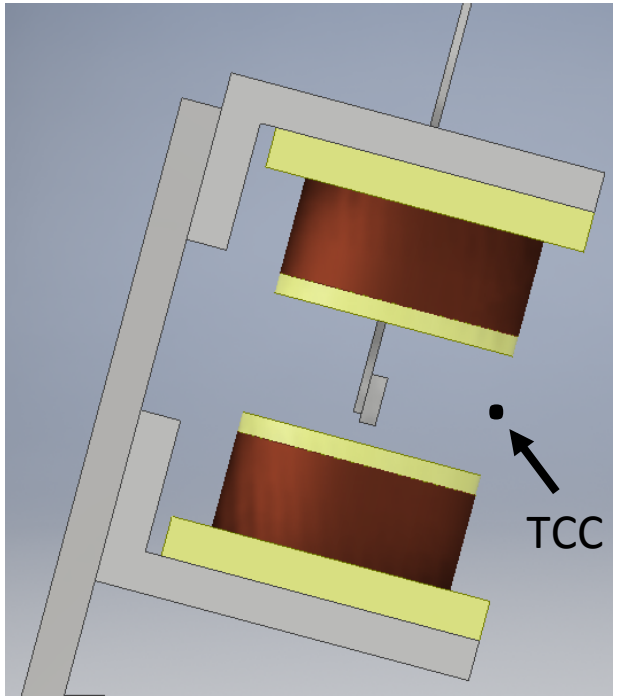

外部磁場印加装置

・青学で設計、九州大・北九州高専で製作。
コイル: 内径=20mm, 外径=30mm, 巻き数20
コイル間距離: 20mm (ホルダ間距離=15mm)
コンデンサ: 3000μF × 4個 (最大電圧800V)。
印加磁場: 電圧400Vで充電。
ショットの瞬間に放電(~5万アンペア)。
B~1.6 T, duration~100 μs

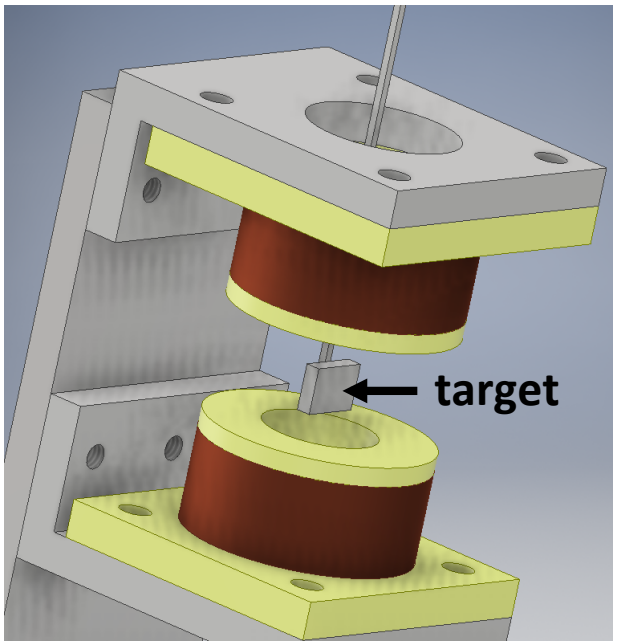

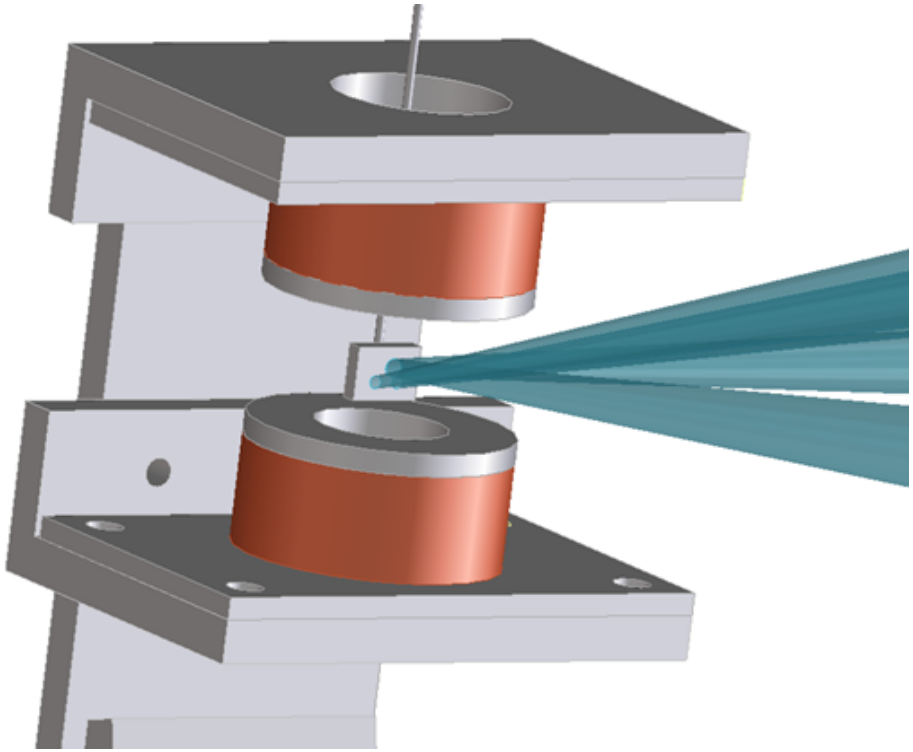

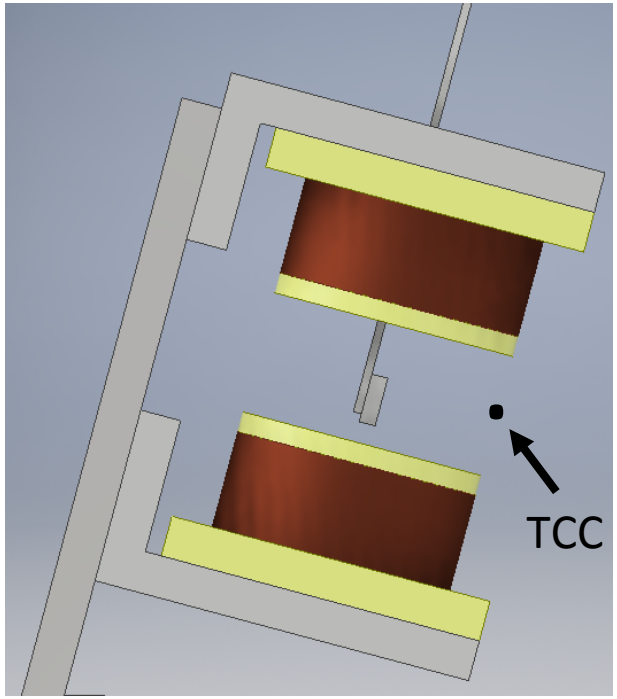

デルリン製のコイルホルダ（白色部分）：北九州高専にて製作。
実験１週間前に完成するも強度不足で大破 => 急遽、アルミ製に変更。

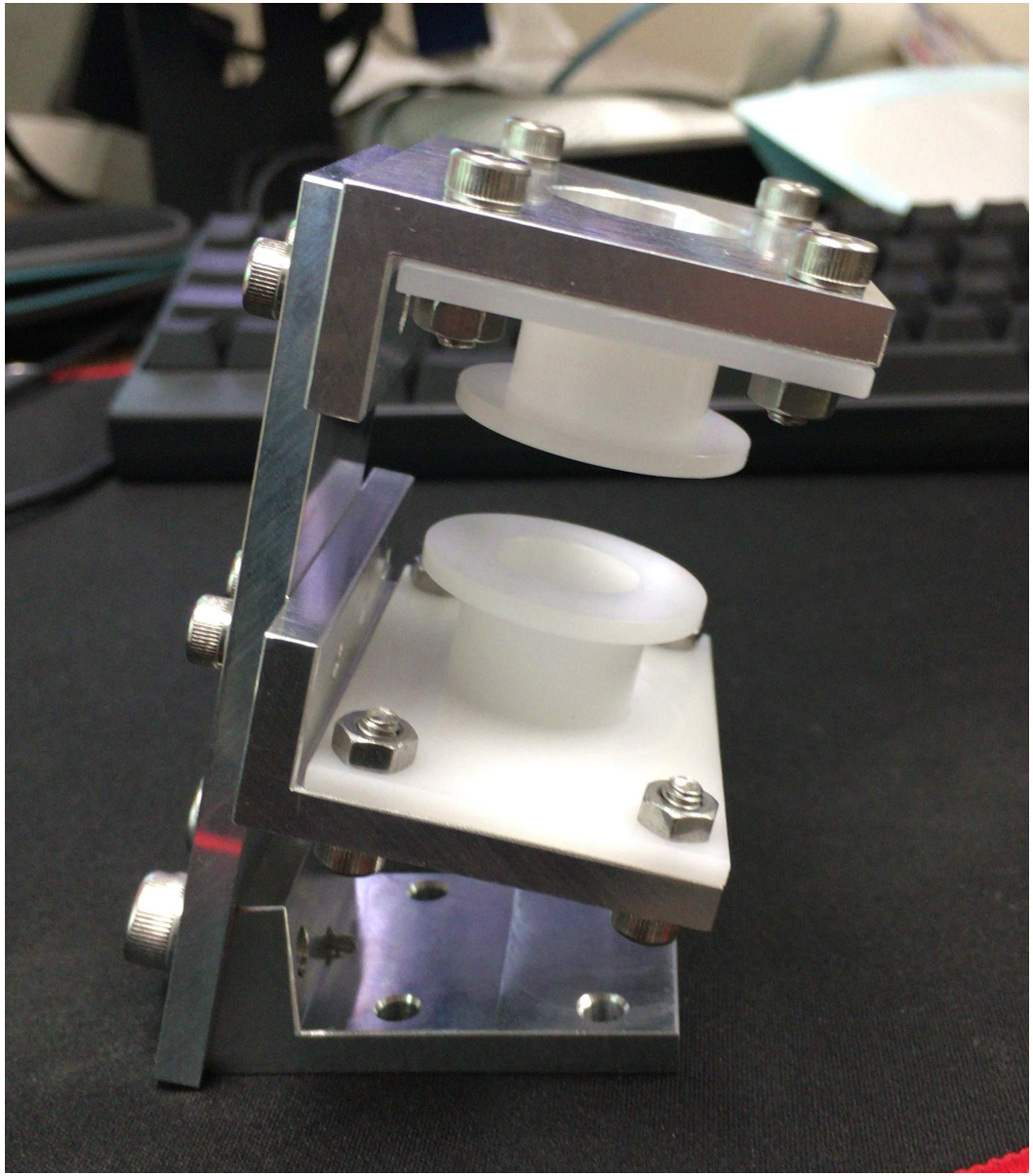

５２番ポート方向から見たコイルとターゲット

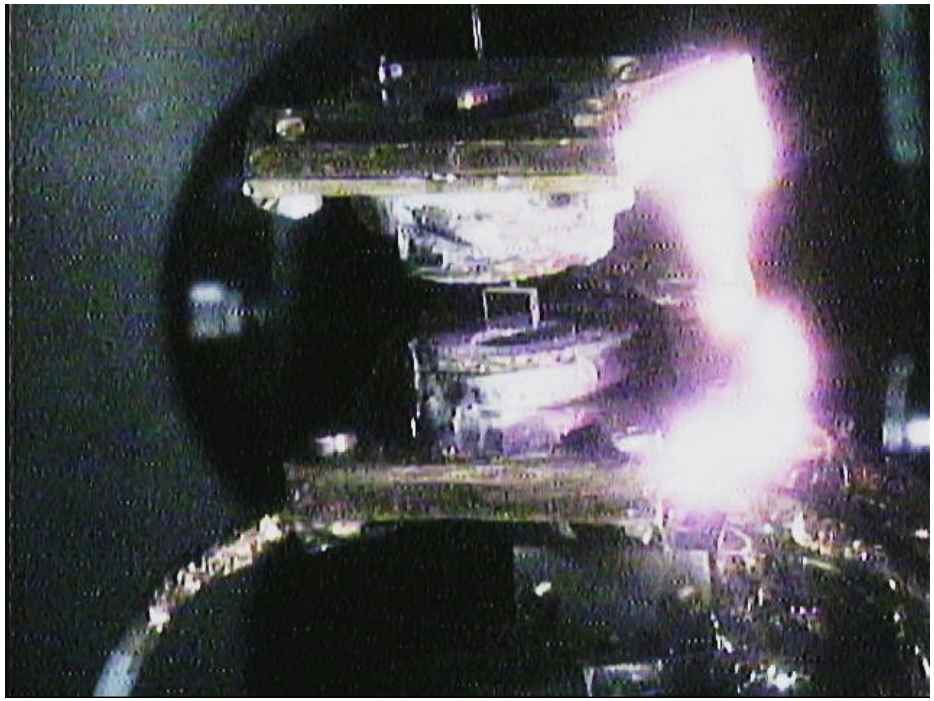

実際の写真

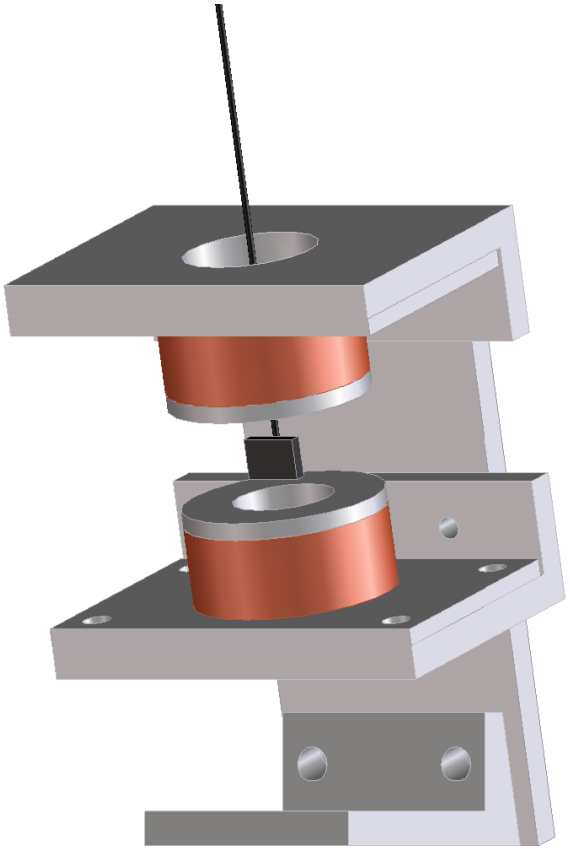

3D CADでの予定

４３番ポート方向から見たコイルとターゲット

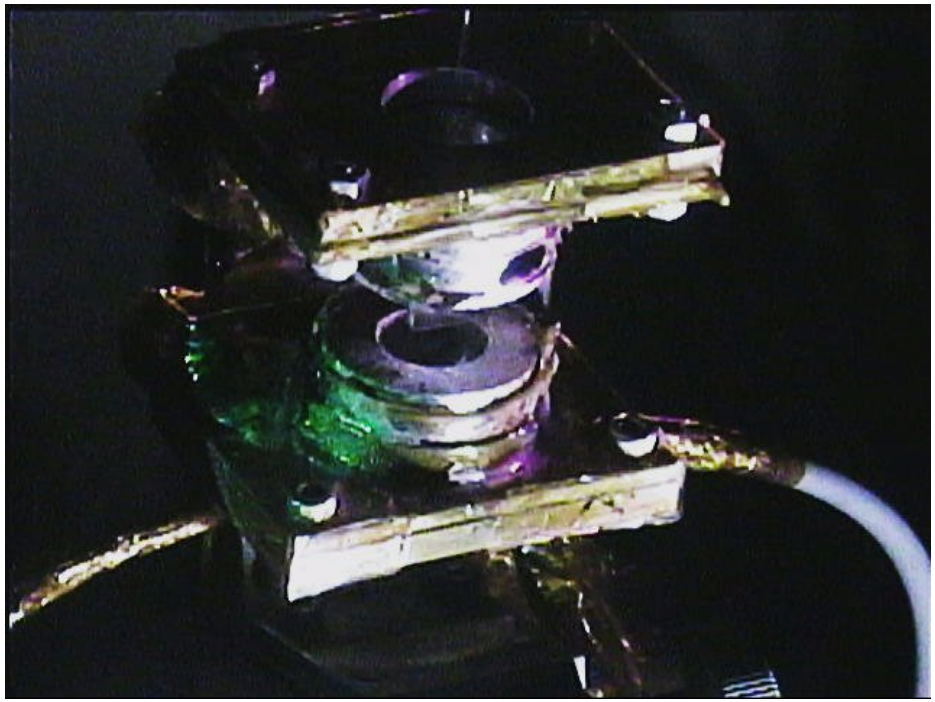

実際の写真

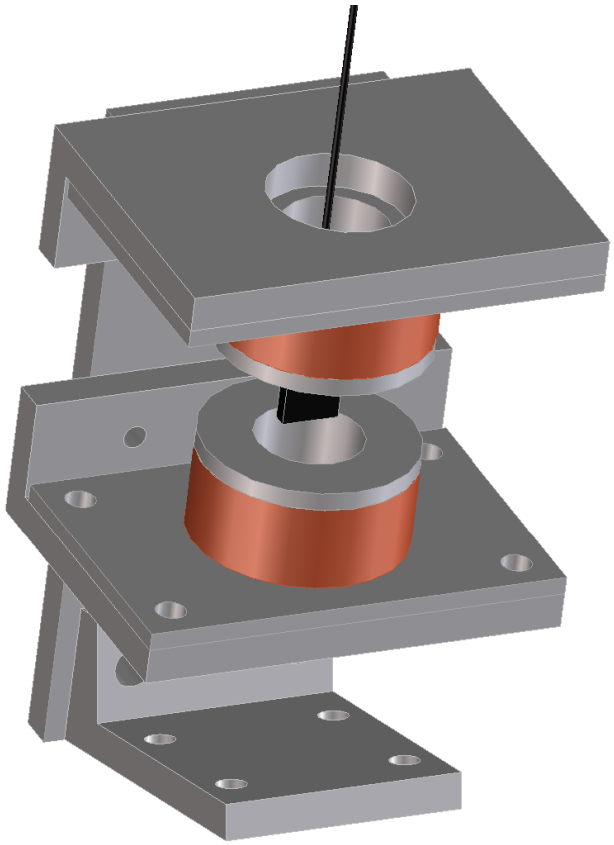

3D CADでの予定

38番ポート方向から見たコイルとターゲット

実際の写真

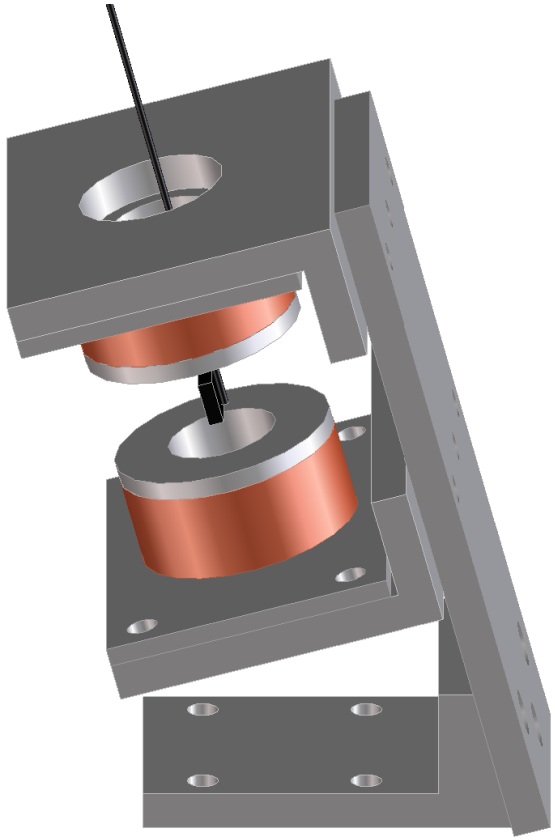

3D CADでの予定

１日（9ショット）使用後のコイルとホルダ治具

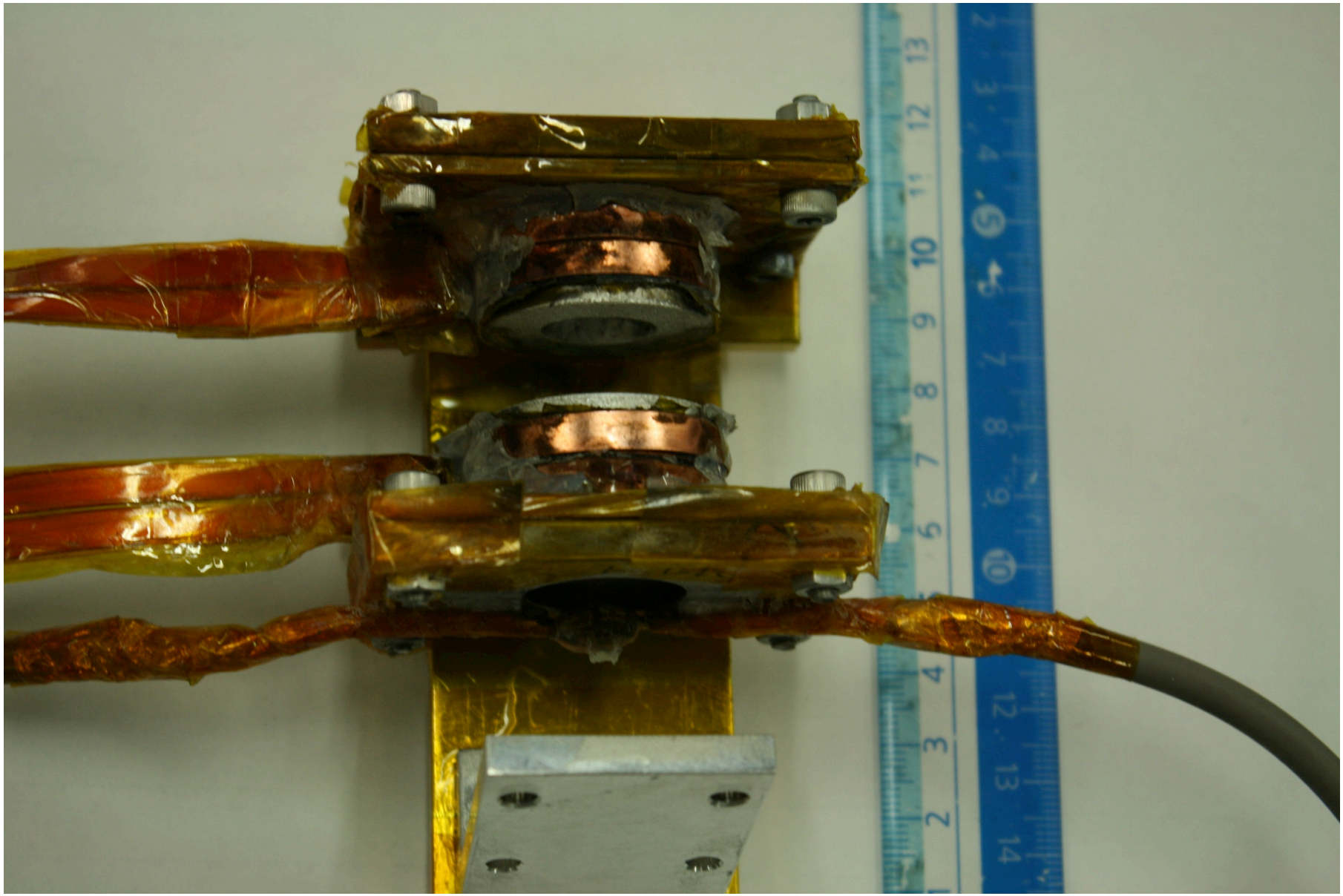

ショット後に回収したターゲット

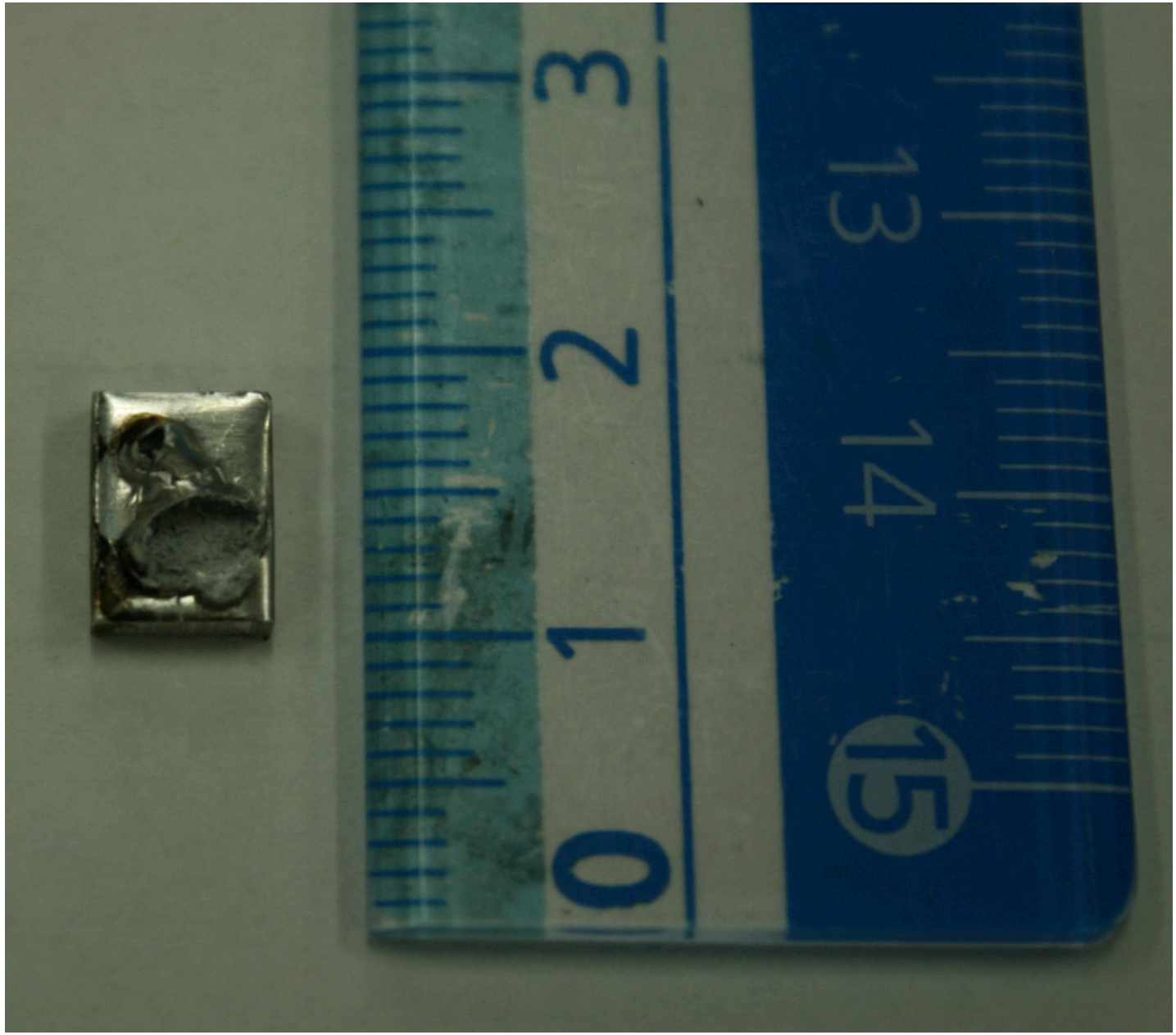

青学チームの分業体制（役割分担）

・青学

山崎：最終方針決定，宿舎予約
田中：自発光ストリーク計測，理論的解釈、方針決定など
遠田(M2)：コイル設計，ターゲット設置，データ解析
宮田(M2)：コイル製作，ターゲット設置，データ解析，トムソン散乱解析コード作成，MHD計算
石坂(M1)：光学計測，データ解析
角地(M1)：コイル設計，ターゲット設置，データ解析
瀬井(M1)：ビアマン磁場計算，線形分散コード作成，データ解析
鈴木(B4)：ターゲット設置，データ解析
河村(B4)：光学計測，ターゲット設置，データ解析，宿舎予約
杉山(B4)：pickupコイル製作，X線pinhole計測，データ解析
冨田(D2)，篠田(M2)，高山(B4)：光学計測

・阪大：共同利用研究の受け入れ

坂和、佐野、太田(M2)、江頭(M2)、和泉(M1)，技士さん達

・九州大

森田，富田：外部磁場印加，トムソン散乱計測，枝本(D1)：外部磁場印加

・その他

大平・松清・大西・蔵満(理論)、梅田(PICシミュレーション)、石井(輻射流体計算)，
竹崎（コイルホルダ製作），米田・浅井・山崎(コイル作成)

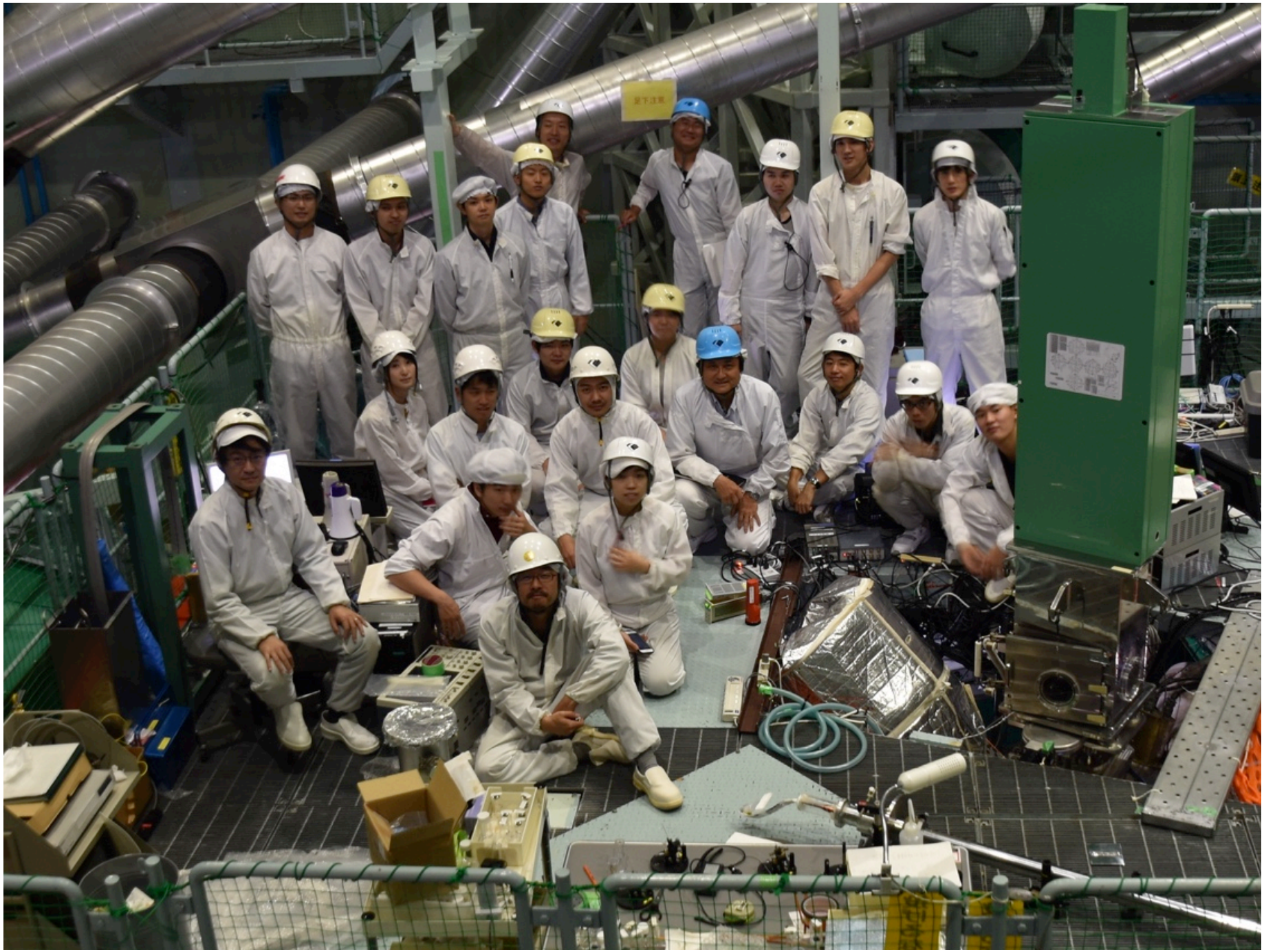

Diagnostics

- Self emission (optical; brems & lines): from high-T regions.
- Shadowgraph : tracing 2nd derivative of n_e.
- Interferometry : tracing n_e
- Collective Thomson scattering : T_e, T_i, n_e, Z, bulk flow velocity
- B-field measurements: B-dot w/ coil, proton backlight

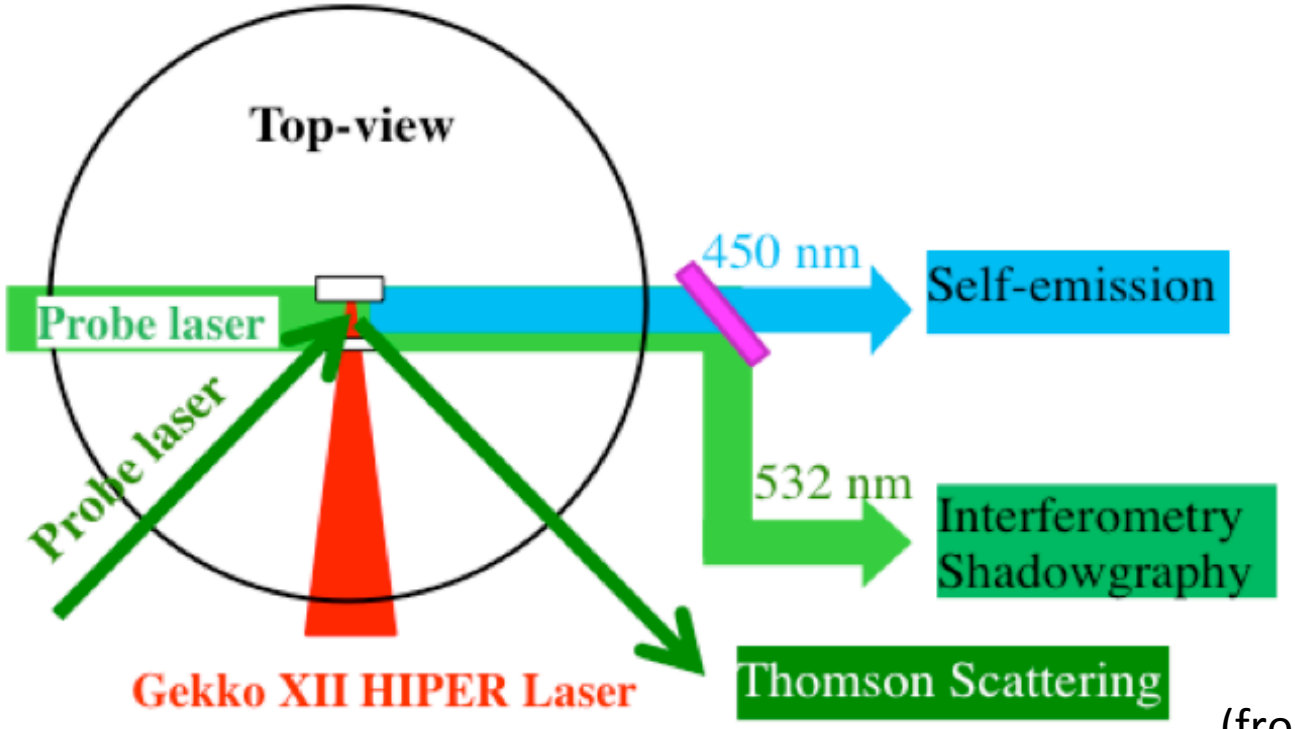

(from Youichi Sakawa)

光学計測の例

Sarkisov (2017), PoP 24, 110701

Optical diagnostics of the exploding hydrated Pd wire with 20.3 μm diameter and 5.2 mm length at 250 ns.

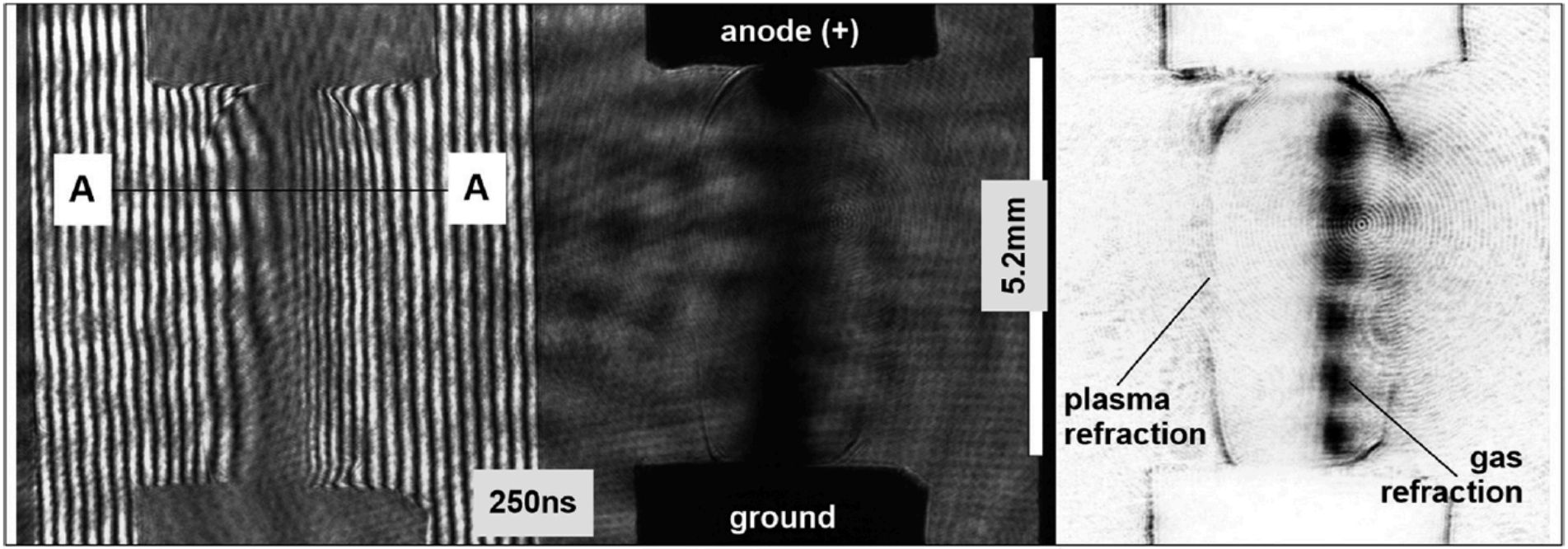

interferogram　　shadowgram　　schlieren

電子密度　　電子密度の2階微分　　電子密度の1階微分

電子密度: $n_e = 10^{16}$~10^{17} cm^{-3}

Schlieren計測

・プローブ光（図の左から入射する平行光）の、
プラズマがない場合の焦点位置 F に尖った障害物（ナイフ・ハサミetc.）を置く。
（つまり、プラズマがない場合は、検出器までプローブ光は届かない。）

・プラズマができるとプローブ光が屈折し、F点を避けて検出器まで届く。

・計測される強度は、イメージ面内で、柱密度のナイフに垂直な方向の
１階微分に比例。=> 密度変化（ジャンプやゆらぎ）を調べるのに便利。

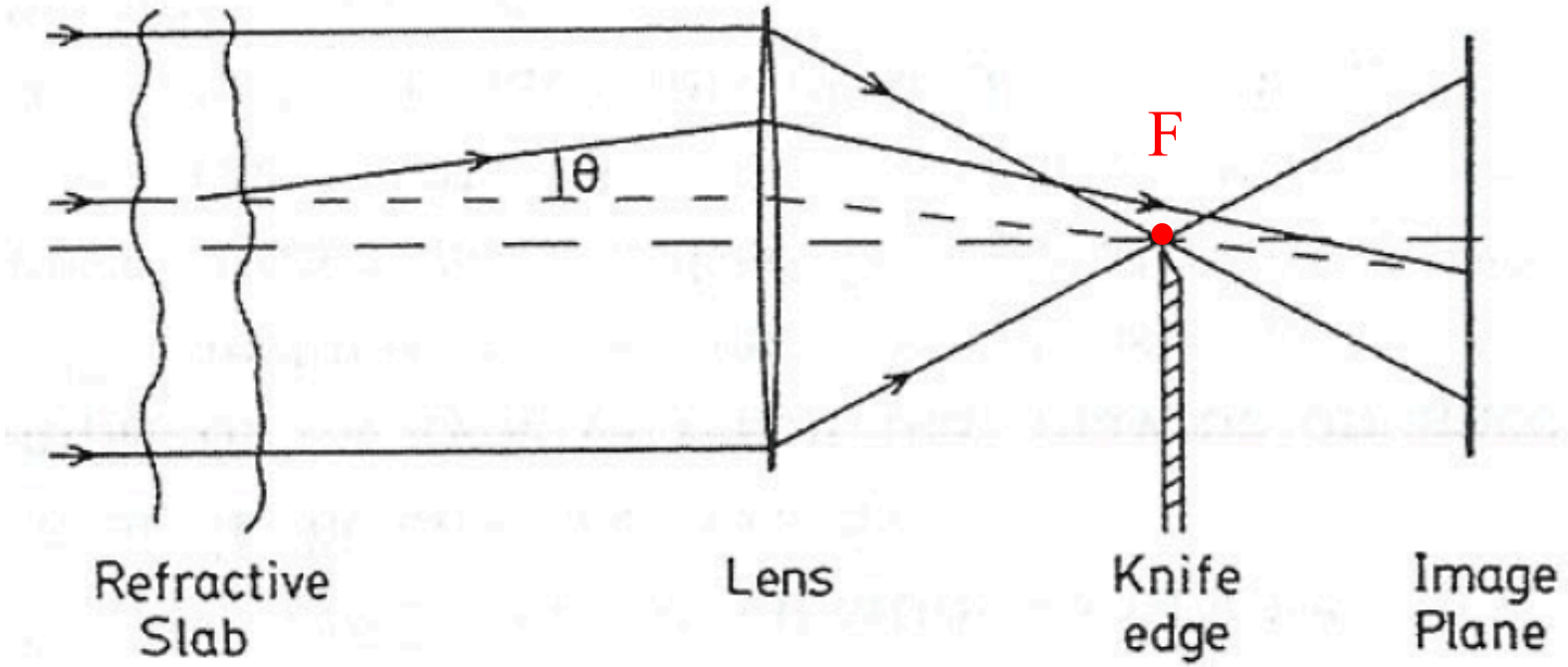

Hutchinson’s textbook

協同トムソン散乱計測

単色光(=532nm)を入射させたときの、協同トムソン散乱スペクトル（右図）：

３つの測定量：
ピーク幅、ピーク間距離、強度の絶対値

４つの知りたい物理量：
イオン温度、電子温度、電子密度、価数。

⇒ 何か1つ条件を課せば
４つの物理量を決定できる。

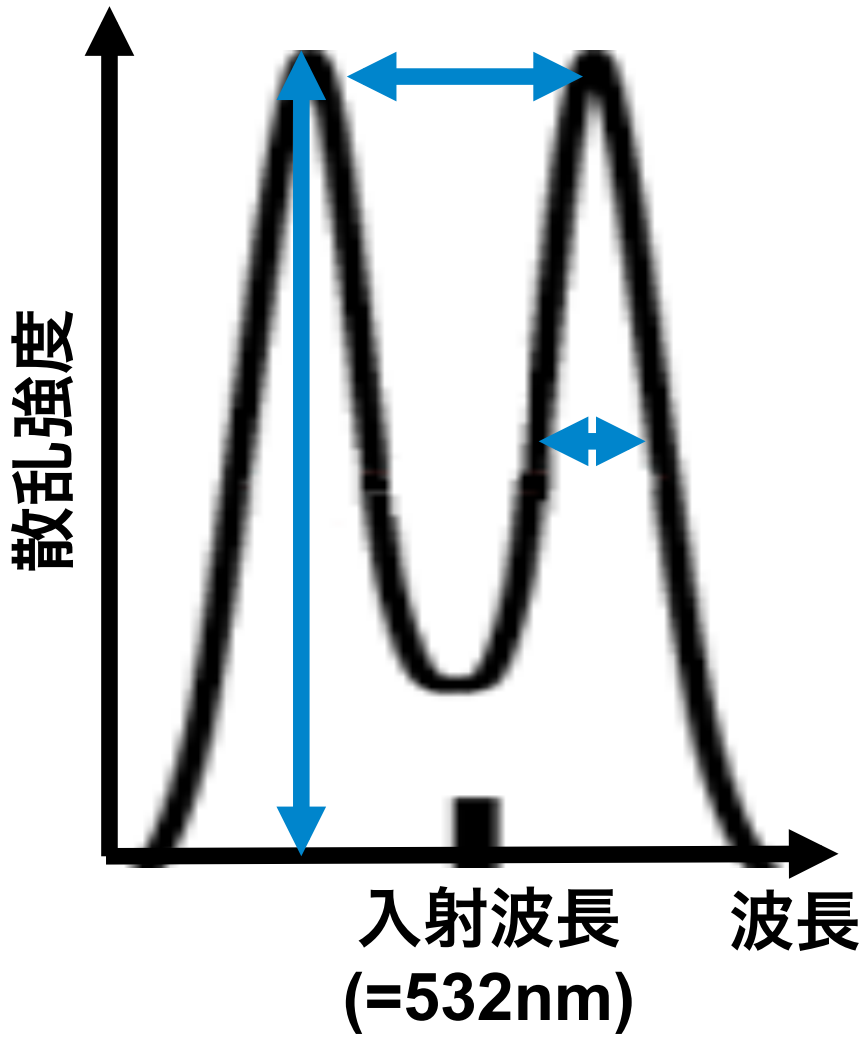

衝撃波遷移層のような非線形性の強いプラズマによる
トムソン散乱光の解析方法は未確立だが、今回の解析では、
プラズマの分布関数をMaxwell分布と仮定。

Preliminary results: B = 0

Thomson scattering (TS) spectrum at TCC (=1.4 cm from target), 17 ns after shot.

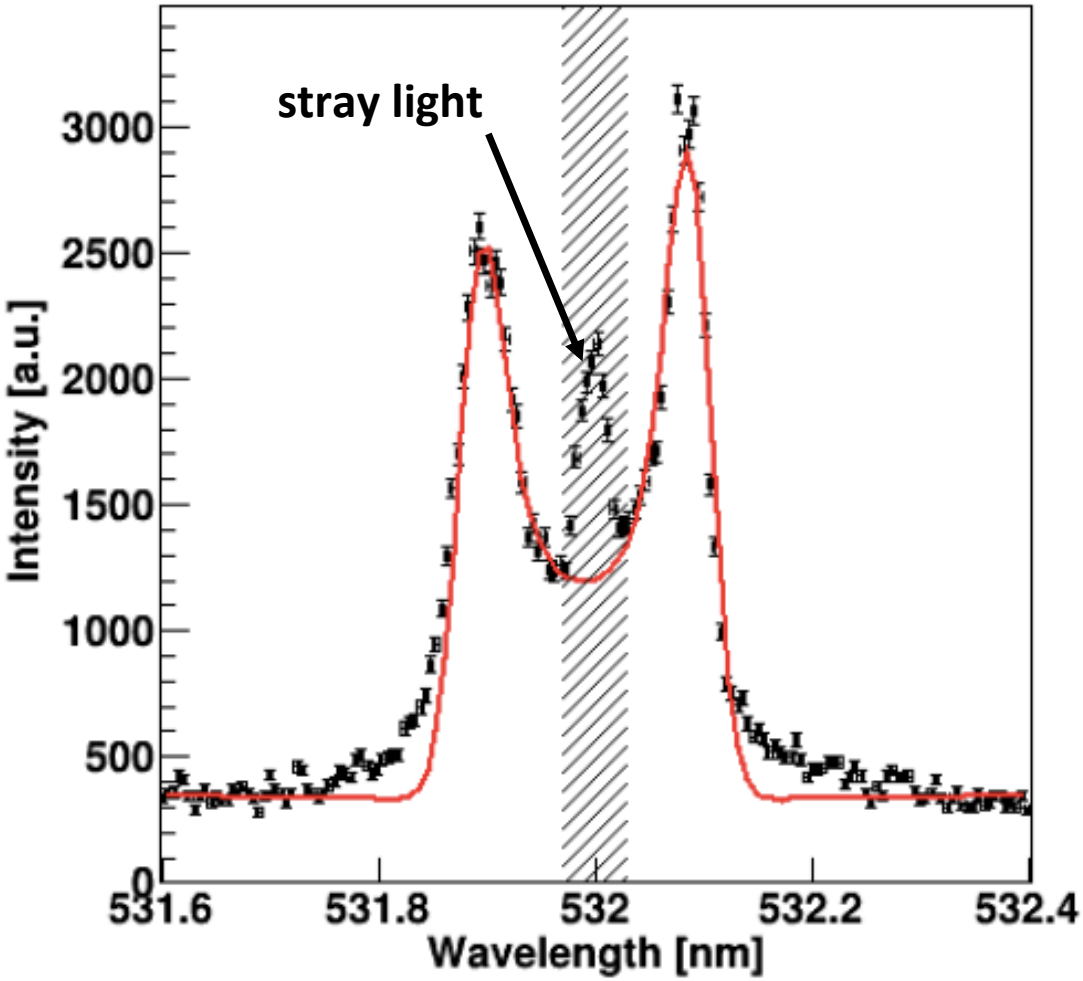

Derived parameters:

$n_e = 1.0\times10^{18}\ cm^{-3}$

$T_e = 94$ eV

$T_i = 30$ eV

$Z = 3.2$

$v_e\text{-}v_i = 150$ km/s,

where we assumed N-gas (5torr) is fully ionized.